Clim. Past, 13, 667–687, 2017
https://doi.org/10.5194/cp-13-667-2017

Climate of the Past
Open Access
EGU

Hydroclimate of the Last Glacial Maximum and deglaciation in southern Australia's arid margin interpreted from speleothem records (23–15 ka)

Pauline C. Treble[1,2], Andy Baker[2], Linda K. Ayliffe[3], Timothy J. Cohen[4], John C. Hellstrom[5], Michael K. Gagan[3], Silvia Frisia[6], Russell N. Drysdale[7], Alan D. Griffiths[1], and Andrea Borsato[6]

[1]Australian Nuclear Science and Technology Organisation, Lucas Heights 2234 NSW, Australia
[2]Connected Waters Initiative Research Centre, UNSW Australia, Kensington 2052 NSW, Australia
[3]Research School of Earth Sciences, Australian National University, Canberra ACT 0200, Australia
[4]School of Earth and Environmental Sciences, University of Wollongong, Wollongong NSW 2522, Australia
[5]School of Earth Sciences, University of Melbourne, Parkville VIC 3052, Australia
[6]School of Environmental and Life Science, University of Newcastle, Callaghan NSW 2308, Australia
[7]School of Geography, University of Melbourne, Parkville VIC 3052, Australia

Correspondence to: Pauline C. Treble (pauline.treble@ansto.gov.au)

Received: 19 December 2016 – Discussion started: 21 December 2016
Accepted: 25 April 2017 – Published: 14 June 2017

Abstract. Terrestrial data spanning the Last Glacial Maximum (LGM) and deglaciation from the southern Australian region are sparse and limited to discontinuous sedimentological and geomorphological records with relatively large chronological uncertainties. This dearth of records has hindered a critical assessment of the role of the Southern Hemisphere mid-latitude westerly winds on the region's climate during this time period. In this study, two precisely dated speleothem records for Mairs Cave, Flinders Ranges, are presented, providing for the first time a detailed terrestrial hydroclimatic record for the southern Australian drylands during 23–15 ka. Recharge to Mairs Cave is interpreted from the speleothem record by the activation of growth, physical flood layering, and $\delta^{18}O$ and $\delta^{13}C$ minima. Periods of lowered recharge are indicated by ^{18}O and ^{13}C enrichment, primarily affecting $\delta^{18}O$, argued to be driven by evaporation of shallow soil/epikarst water in this water-limited environment. A hydrological driver is supported by calcite fabric changes. These include the presence of laminae, visible organic colloids, and occasional dissolution features, related to recharge, as well as the presence of sediment bands representing cave floor flooding. A shift to slower-growing, more compact calcite and an absence of lamination is interpreted to represent reduced recharge.

The Mairs Cave record indicates that the Flinders Ranges were relatively wet during the LGM and early deglaciation, particularly over the interval 18.9–15.8 ka. This wetter phase ended abruptly with a shift to drier conditions at 15.8 ka. These findings are in agreement with the geomorphic archives for this region, as well as the timing of events in records from the broader Australasian region. The recharge phases identified in the Mairs Cave record are correlated with, but antiphase to, the position of the westerly winds interpreted from marine core MD03-2611, located 550 km south of Mairs Cave in the Murray Canyons region. The implication is that the mid-latitude westerlies are located further south during the period of enhanced recharge in the Mairs Cave record (18.9–16 ka) and conversely are located further north when greater aridity is interpreted in the speleothem record. A further comparison with speleothem records from the northern Australasian region reveals that the availability of tropical moisture is the most likely explanation driving enhanced recharge, with further amplification of recharge occurring during the early half of Heinrich Stadial 1 (HS1), possibly influenced by a more southerly displaced Intertropical Convergence Zone (ITCZ). A rapid transition to aridity at 15.8 ka is consistent with a retraction of this tropical moisture source.

Published by Copernicus Publications on behalf of the European Geosciences Union.

1 Introduction

Evidence in the paleoclimate record for the nature and timing of changes in the Australian environment at the time of HS1 can assist in the critical assessment of how the climate system reacts to complex feedbacks in the ocean and atmosphere system (Clark et al., 2012). However, little is currently known about the impact of Heinrich stadials on Australian climate, and the Southern Hemisphere mid-latitudes in general, as reliable terrestrial paleoclimate records from this region are sparse (Broecker and Putnam, 2012). The latitudinal position of the westerly winds at the Last Glacial Maximum (LGM) is also an important research question which still remains debated despite long-running attention, both specifically in the southern Australian sector (Bowler, 1978; Bowler and Wasson, 1984; Wywroll et al., 2000; Shulmeister et al., 2004, 2016; Williams et al., 2009; Hesse et al., 2004; Turney et al., 2006; Haberlah et al., 2010; Cohen et al., 2011; De Deckker et al., 2012) and elsewhere in the Southern Hemisphere (Gasse et al., 2008; Kohfeld et al., 2013; Sime et al., 2013).

Currently, only a single proxy record exists from within the Australian sector for the position and strength of the westerly winds during the LGM and deglaciation (De Deckker et al., 2012). Marine core MD03-2611 (33–10 ka) (Fig. 1a) is located east of the Great Australian Bight in the Murray Canyons region at the present position of the subtropical front (STF). The paleo-position of the STF is interpreted from the foraminifera micro-fossil record (*Neogloboquadrina pachyderma* dextral), which in turn is used to infer the position and strength of the westerly winds (De Deckker et al., 2012). Several latitudinal excursions of the westerlies, relative to their Holocene position, were interpreted from this record, including a northward displacement of the westerlies during the peak of the LGM and a southward displacement during HS1 (De Deckker et al., 2012). A key assumption of the study by De Deckker et al. (2012) is that the position of the westerly winds coincides with the position of the oceanic STF, which may be a potential shortcoming (e.g. de Boer et al., 2013). A way of further assessing this interpretation is to examine the hydrological response to latitudinal shifts in the westerly winds in the terrestrial record of southern Australia.

Southern Australia is presently dominated by semi-arid drylands that skirt the southern margin of Australia's arid interior. The proximity to the arid interior means that it is hydrologically sensitive to episodes of climatic change (Fitzsimmons et al., 2013). Terrestrial data that span the LGM and the subsequent deglaciation are particularly sparse in this region and limited to discontinuous sedimentological and geomorphological archives (e.g. salt lakes, dune systems, ephemeral fluvial systems). Such records typically carry large chronological uncertainties due to preservation issues (e.g. lack of organic material, reworking of sediments, erosion) as well as the limitations of applicable age measurement techniques (Fitzsimmons et al., 2013). Additionally, the interpretation of geomorphic records may not be straightforward for other reasons. For example, dune activation may respond non-linearly to precipitation and be a function of sediment supply as well as aridity (Fitzsimmons et al., 2013), whilst the generally large catchments of Australia's arid interior contribute uncertainty over whether fluvial systems are recording local or distal conditions. For example, Lake Frome receives water from a catchment of nearly 63 000 km^2, with 44 % of this contributing area drained by the adjacent Flinders Ranges and the rest from the adjacent dunefields (Cohen et al., 2012). Furthermore, connections with lakes Blanche and Callabonna mean that when Strzelecki Creek flows (via the tropically sourced Cooper Creek) the contributing area of Lake Frome can actually be > 363 000 km^2.

Speleothems offer a number of advantages over the geomorphic archives described above, including being recorders of local recharge due to a relatively small catchment, and typically being well preserved in stable cave environments. Speleothems also yield precise and accurate chronologies based on U-series age measurements that typically result in age uncertainties of < 1 % (2σ; Hellstrom, 2003). The construction of highly resolved (sub-decadal) climatically sensitive geochemical records spanning 10^3–10^4-year timescales has also been achieved (e.g. Wang et al., 2001; Griffiths et al., 2016). For example, over glacial–interglacial transitions in monsoonal climates, they have been particularly successful in revealing the timing and structure of ice age terminations (Cheng et al., 2010) and have placed speleothems at the forefront of chosen tools for paleoclimate reconstruction (Henderson, 2006; Fairchild and Baker, 2012).

Cave monitoring studies have shown dripwater $\delta^{18}O$ to be primarily a function of rainfall $\delta^{18}O$ in non-arid environments (e.g. Fuller et al., 2008; Moerman et al., 2014; Riechelmann et al., 2011; Treble et al., 2013; Duan et al., 2016), although the complexity of the response of the speleothem $\delta^{18}O$ signal to climate is also recognised owing to karst hydrological pathways (Baker and Brunsdon, 2003; Treble et al., 2013), recharge thresholds (Pape et al., 2010; Markowska et al., 2015), and in-cave effects, including disequilibrium during degassing (due to evaporation) and ventilation effects (e.g. Pape et al., 2010; Feng et al., 2012; Deininger et al., 2012; Cuthbert et al., 2014a, b; Riechelmann et al., 2013; Dreybrodt and Deininger, 2014; Rau et al., 2015).

Cave monitoring studies and speleothem records in general are primarily focused on temperate or tropical environments. Far less monitoring has been undertaken within semi-arid/arid climates (with the exception of Ayalon et al., 1998; Pape et al., 2010; Cuthbert et al., 2014a, b; Markowska et al., 2016). In these drier landscapes, where there is less frequent recharge, and temperatures conducive to evaporation occur, one would expect evaporative processes to increasingly affect dripwater $\delta^{18}O$, and hence speleothem $\delta^{18}O$, with increasing aridity. Speleothem growth itself is typically episodic within semi-arid climates (Ayliffe et al., 1998; Wang et al.,

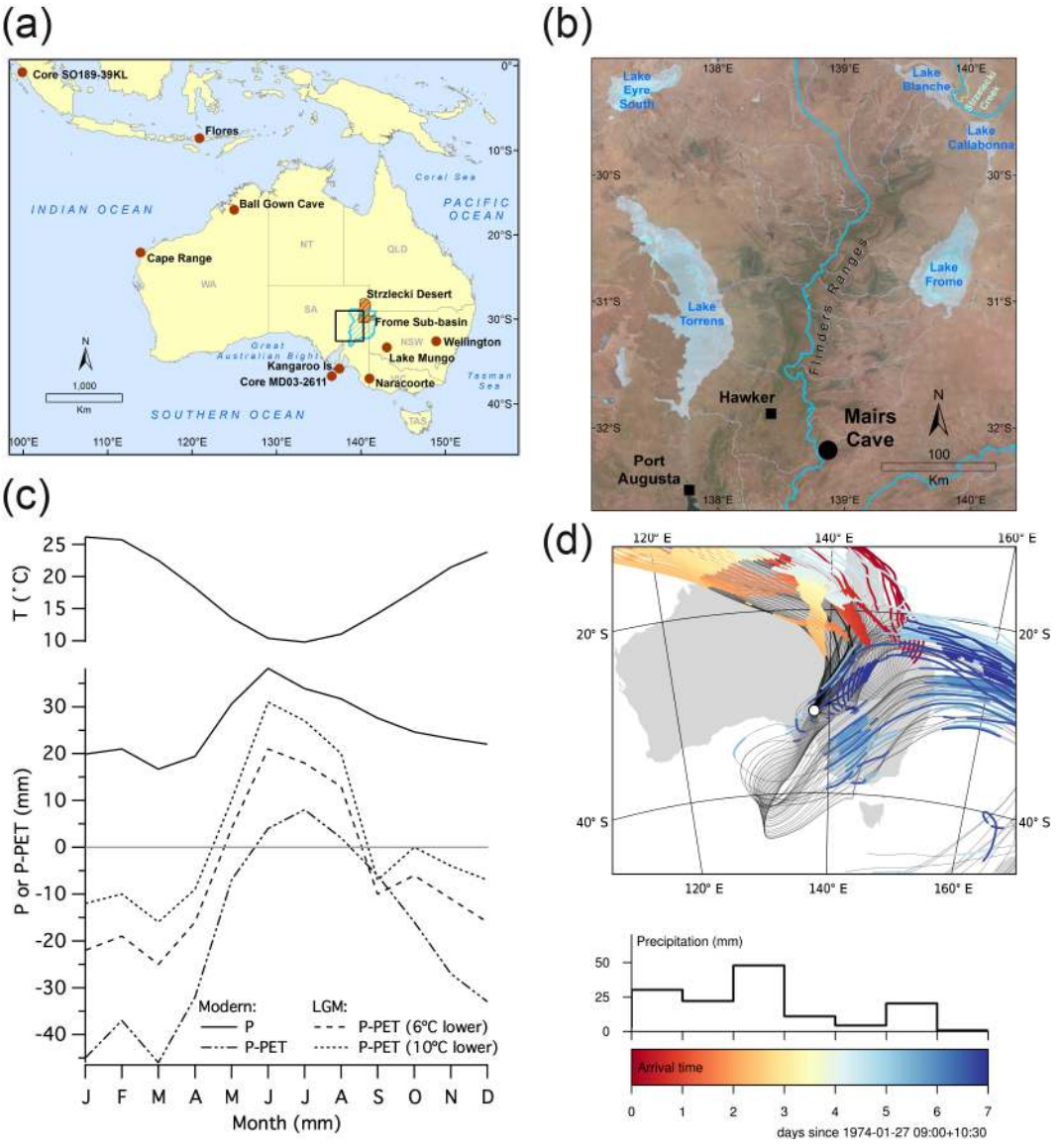

Figure 1. Location of the Flinders Ranges and other sites described in the text **(a)**; location of Mairs Cave, Flinders Silts, and Lake Frome **(b)**; monthly climate statistics for Hawker (approximately 60 km from Mairs Cave) and hydrologically effective precipitation or P-PET calculated using the Thornthwaite method for modern-day and LGM scenarios of 6 or 10 °C temperature cooling **(c)**; and air mass back trajectories for 27 January to 3 February 1974 (upper panel) and daily precipitation (lower panel) **(d)**. Back trajectories are 10 days long, ending at Mairs Cave and 1500 m a.g.l. Meteorological forcing is derived from the 2.5° NCEP/NCAR Reanalysis (Kalnay et al., 1996). Trajectories are colour-coded according to arrival time but only during intervals when the air mass is beneath the surface boundary layer to indicate potential moisture sources – i.e. we interpret the source of moisture for air masses arriving between days 4 and 7 to be the Pacific (below boundary layer) rather than the Southern Ocean (above boundary layer). Precipitation is the average of 13 stations within 50 km of Hawker.

2004; Vaks et al., 2006; Stoll et al., 2013). Recent studies from Wellington Caves (Fig. 1a) in semi-arid central New South Wales, Australia, have contributed substantially to a process-based understanding of the climate-speleothem signal in water-limited environments. Cuthbert et al. (2014a, b) showed that evaporation of water held in shallow karst stores, occurring in between recharge events, resulted in ^{18}O enrichment of dripwater by several per mil. It has also been shown that significant recharge thresholds need to be overcome to replenish karst water stores at this semi-arid site (Markowska et al., 2016). These processes are likely to amplify the dripwater isotopic response to infiltration events, as well as introduce potential biases in the preservation of rainfall events depending on their frequency and magnitude. On the whole, speleothem records from water-limited systems can be expected to have a considerable range in isotopic values, as well

as a heightened non-linear relationship between climate and the speleothem isotopic record (Cuthbert et al., 2014a). In this context, they thus should be viewed as a record of paleo-recharge rather than a direct proxy of paleo-rainfall.

There has been relatively little use of speleothem records to reconstruct southern Australia's dryland history. To date, just three speleothem stable isotope records exist for this region (Desmarchelier et al., 2000; Bestland and Rennie, 2006; Quigley et al., 2010) from marine isotope stages 6 and 5d, and the Holocene, but all are of particularly low-resolution and contain lengthy millennial-duration hiatuses. Previous research has produced age measurements of speleothems from caves in this region resulting in age–frequency histograms for Naracoorte Caves, the Flinders Ranges, and Kangaroo Island (Fig. 1a) (Ayliffe et al., 1998; St Pierre et al., 2012; Cohen et al., 2011, 2012). These studies highlight that speleothem growth in the southern margin of Australia's drylands is primarily a function of water balance, with enhanced speleothem growth coinciding with intervals of potentially greater moisture availability (Ayliffe et al., 1998; St Pierre et al., 2012; Cohen et al., 2011; Fitzsimmons et al., 2013). For example, the first such study by Ayliffe et al. (1998) demonstrated that speleothem growth at Naracoorte Caves is more frequent in the stadial periods of the last glacial cycle. This was attributed to increased effective precipitation as a result of reduced evaporation (Ayliffe et al., 1998).

A more recent study highlighted the climatic relationship between speleothem growth and pluvial intervals in this region via the overlap of two stalagmite records from Mairs Cave in the Flinders Ranges with lake-full conditions at Lake Frome. Lake Frome is 200 km NE of the cave site and is fed by run-off from the eastern slopes of the Flinders Ranges (Cohen et al., 2011). This relationship between enhanced speleothem growth during periods of increased effective precipitation is also observed outside Australia (e.g. Wang et al., 2004; Vaks et al., 2006; Stoll et al., 2013) and highlights stalagmite growth as a useful on/off indicator of recharge in semi-arid to arid environments.

In this study, we present the geochemical records of these two stalagmites from Mairs Cave. As it was not practical to monitor Mairs Cave owing to its remote location, lack of active dripwater, and infrequent recharge, we compare our data with the modern analogue study at Wellington Caves, in a temperate semi-arid environment 1000 km NE of Mairs Cave (Fig. 1a). We also draw on a comparison of our data with independent evidence for the location of the westerly winds, inferred from the foraminifer-derived proxy record of the STF from marine core MD03-2611 (De Deckker et al., 2012) and tropical speleothems from northern Australasia (Ayliffe et al., 2013; Denniston et al., 2013a, b) as well as other archives of climatic change relevant to the southern Australian region.

2 Regional setting

Today, the Flinders Ranges and surrounding region are classified as semi-arid to arid, and speleothem growth in the isolated pockets of Cambrian-age limestone karst is very sparse. The Flinders Ranges are a rugged 400 km long topographic divide intercepting the path of the westerly winds from the Southern Ocean, providing orographically enhanced rainfall in a region otherwise characterised by flat, arid dunefields and large salt lakes (Fig. 1a, b).

Rainfall at Mairs Cave is predominantly derived during the austral winter months (Fig. 1c) but recharge in typical years is small to negligible, explaining the lack of modern speleothem growth. The region experiences limited connectivity with tropical moisture sources, owing to its position on the southern limb of the Hadley cell, although the development of continental troughs during summer months can favour advection of moisture from the eastern Indian Ocean or Coral Sea and generate heavy summer rains (Schwerdtfeger and Curran, 1996; Pook et al., 2014). In a study of the synoptic climatology of heavy rainfall ($>25\,\mathrm{mm\,day^{-1}}$) at Lake Frome over the period 1950–2014 ($n = 25$), Pook et al. (2014) demonstrated that 53 % of these events involved tropical and/or a pre-existing subtropical cloudband and that 90 % of the events occurred when the Southern Oscillation index was in a positive (towards La Niña) phase.

The 1974 CE filling of Lake Frome and Lake Callabonna (Fig. 1b) is one of the most significant hydrological episodes in the historical record and happened in a year when a La Niña also coincided with a negative Indian Ocean Dipole (IOD) event. Negative IOD events occur when sea surface temperatures in the eastern tropical Indian Ocean are warmer than average, feeding moisture into Australia's interior (Risbey et al., 2009). The lakes were fed both by direct runoff from the Flinders Ranges and from rain further north, via Strzelecki Creek (Cohen et al., 2011, 2012). During a single week-long event, rainfall records were broken across much of the arid interior. Persistent rainfall was generated by sustained moist tropical airflow. Eighty percent of the resulting rainfall came from the eastern Indian Ocean during the first 4 days before switching to the western Pacific Ocean, as shown by trajectory analysis (Fig. 1d).

Mairs Cave

Mairs Cave (138°50′ E, 32°10′ S; Fig. 1b) is located in Buckalowie Gorge in the central Flinders Ranges. The cave is developed along three parallel bedding planes in the limestone (Kraehenbuehl et al., 1997). Its overall length is 400 m, although the main chamber is 120 m long by 10 m wide, accessed via a 17 m vertical pitch at the cave entrance (Kraehenbuehl et al., 1997). Mairs Cave contains both coffee-coloured and clean white speleothems. Bands of coffee-coloured stalagmites lie underneath limestone joints, many overgrown with clean white formation.

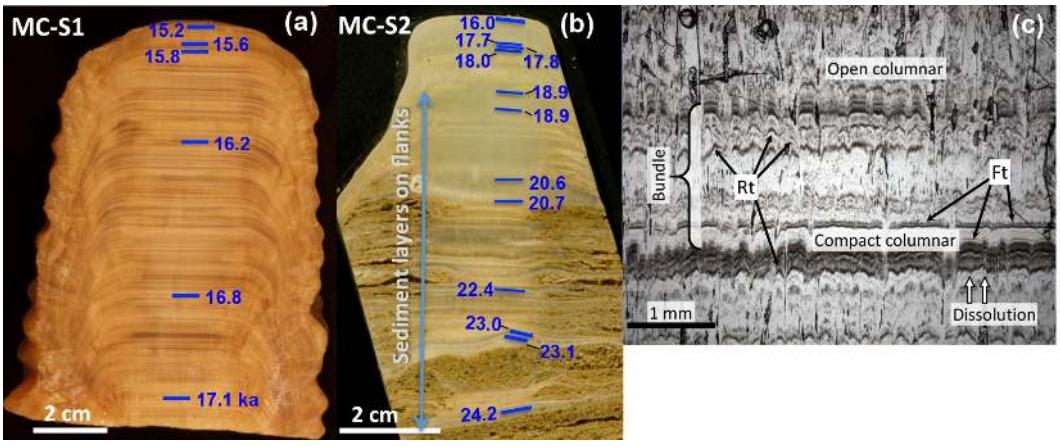

Figure 2. Mairs Cave stalagmites MC-S1 **(a)** and MC-S2 **(b)** with age measurements (ka) indicated. Photograph of thin section from MC-S1 showing parallel laminae **(c)**. See Sect. 4.2 for description of features in thin section. MC-S2 contains layers of sediment interbedded with calcite lenses in its lower half. Sediment continues to be visible on the side flanks until 25 mm below the top, coinciding with the age measurement of 18.9 ka. White annulus in layer over 20.6 ka age measurement is a sectioned bone.

3 Materials and methods

The two stalagmites used in this study were collected from Mairs Cave (Fig. 1b) in 1998 CE. MC-S1 was collected from the main chamber ∼ 100 m into the cave and MC-S2 from a side chamber located ∼ 20 m from the vertical shaft forming the cave entrance. There is evidence of flooding in the lower parts of Mairs Cave including calcite deposits in rims indicating former pool levels. In addition, cavers report 3 m of water in the entrance shaft in 1974 after the particularly heavy period of rain described in Sect. 2 (Kraehenbuehl et al., 1997). There is no geomorphic evidence of streamflow inside the cave. The base of the entrance shaft is presently at a similar level to the creek flowing through Buckalowie Gorge but floodwaters are unlikely to be delivered to the cave via overbank flow from rising creek levels, as they would have to overtop > 15 m, which seems unlikely given the broad cross-section of the valley at this location. Alternatively, flooding may be caused by runoff from the steep terrain above the cave entrance. Judged from the cave maps (Hill, 1958), MC-S2 was located 30 m from and at a similar depth to the base of the entrance shaft. MC-S2 was thus likely to have been inundated during the 1974 flood event. In contrast, MC-S1 grew ∼ 4 m higher in elevation.

3.1 Description of stalagmites

The two stalagmites are considerably different in appearance (Fig. 2a, b). MC-S1 is darker "coffee-coloured" (Fig. 2a) and contains well-defined parallel laminae appearing throughout the specimen (Fig. 2c), consisting of columnar and open-columnar fabric (Frisia et al., 2000). The growth surface of MC-S1 was wide and flat-topped, with gour features along the stalagmite flanks indicative of high dripwater Ca concentrations and high drip rate. The coffee colour is also indicative of organics, which would suggest greater connectivity to the soil than MC-S2. MC-S1 was sawn from a flowstone-covered boulder. Approximately 10–15 mm of its base was not recoverable owing to the saw cut.

Stalagmite MC-S2 is pale, semi-translucent, and forms a narrow candle-stick stalagmite in its upper half. It contains thin lenses of calcite alternating with layers of calcified sediment in the lower half (Fig. 2b). This lower section captures the earliest growth phase of MC-S2, when calcite deposition competed with aggradation of sediment on the floor of the cave where MC-S2 grew (Fig. 2b). These sediment layers, assumed to be deposited by floodwaters, are more prominent and thicker in the lowest half of MC-S2, but are still visible on the stalagmite flanks between ∼ 25 and 45 mm below the top. Sediment layers above this (upper 25 mm) appear to be absent, suggesting that either (i) sediment became more efficiently washed from the surface of MC-S2 as the morphology of its flanks became increasingly steeper or (ii) a cessation in sediment delivery by floodwaters. The differences in the morphology of the two stalagmites indicate that this may be a function of drip rate: while both stalagmites are flat-topped with parallel bands, MC-S1 is twice as wide and has distinctive gour features on its sides, more commonly seen in flowstone, and indicative of higher drip rate (Baldini, 2001). The different morphologies also indicate individual hydrological flow paths which can impact the geochemical record also (e.g. Bradley et al., 2010).

3.2 Methods

Two 5 mm slabs were sectioned longitudinally from each stalagmite. One slab was further sectioned along the longitudinal axis for stable isotopes and trace element analyses, while the ∼ 8 mm wide portion from the central axis of the second slab was removed for age measurements. Calcite wafers, typ-

ically 1–2 mm thick, were further subsampled for age measurements. Adjacent surfaces were utilised to minimise potential offsets in the depths of measurement transects for stable isotope, trace element, and age measurements.

Powders were obtained for stable isotope analysis via continuous micro-milling at 300 and 100 µm for MC-S1 and MC-S2 respectively, yielding sub-decadal resolution (approximately 5 years for the majority of each stalagmite; milling dimensions parallel to laminae were 2×2 mm for MC-S1 and 2×4 mm for MC-S2). The earliest visible lens of MC-S2 growth (Fig. 2c) was not included in the isotopic record owing to chronological uncertainty for this part of the record and detrital contamination (see Sect. 4.1). Speleothem MC-S1 powders were analysed for $\delta^{18}O$ and $\delta^{13}C$ on a Finnegan MAT251 at the Research School of Earth Sciences (RSES), Australian National University, whilst MC-S2 powders were run on a GV2003 continuous-flow IRMS at the University of Newcastle. Data are normalised to the Vienna Pee Dee Belemnite (VPDB) scale using NBS-19 ($\delta^{18}O = -2.20$ ‰ and $\delta^{13}C = +1.95$ ‰) and NBS-18 ($\delta^{18}O = -23.0$ ‰ and $\delta^{13}C = -5.0$ ‰). The long-term measurement precision for NBS-19 at RSES is 0.07 ‰ (2σ) for $\delta^{18}O$ and 0.04 ‰ (2σ) for $\delta^{13}C$. Reproducibility between instruments was cross-checked by running aliquots of 15 MC-S1 powders on each instrument resulting in < 0.2 ‰ offset ($\delta^{18}O$ and $\delta^{13}C$). Initially every third sample was run and subsequent analyses were run to in-fill the time series as necessary. Spectral analysis of $\delta^{18}O$ data was performed using the Lomb–Scargle method for unevenly sampled data (Press and Rybicki, 1989).

Trace elements were analysed by laser ablation inductively coupled plasma mass spectrometry (LA-ICPMS) at RSES using a 193 nm excimer laser masked by a slit that resulted in a rectangular area ablated from the sample surface that was 120 µm wide and 40 µm high aligned with the narrower dimension in the direction of speleothem growth. The sample was moved underneath the laser on a motorised stage at 2 mm min^{-1} while the laser was pulsed at 20 Hz such that the laser "scanned" along the central growth axis of the speleothem. The ablated material was carried to an Agilent 7500 s quadrupole ICPMS and the elements Ca, Mg, Sr, U, Al, and Si analysed and standardised to NIST 612 concentrations (Mg: 85.09; Sr: 78.4; Al: 10 588; U: 37.88 ppm; Pearce et al., 1996). Full details of the LA-ICPMS procedure and data reduction are given in Treble et al. (2003). Construction of a proxy record of the sedimentary layers using Al and Si concentrations was attempted, but this was not successful due to the uneven distribution of sediment across the layers, and the tendency for sediments to be present on the stalagmite flanks rather than the axis. Instead, the location of sediment bands was identified in thin section.

Petrographic observations were carried out on uncoated, polished thin sections under plane (PPL) and cross-polarised light (XPL) using a Zeiss Axioskop optical microscope and a Leica MZ16A stereomicroscope at the University of Newcastle. Fabrics were coded following a conceptual framework proposed in Frisia (2015), which is based on models of fabric development as a response to changes in cave environmental parameters. The changes of fabrics through time were obtained by assigning numbers to each fabric recognised in the stalagmites and plotting their variability along the vertical axis (with respect to distance from top). In this conceptual framework (see Frisia et al., 2000; Frisia, 2015), number 1 is assigned to clean, columnar calcite. The highest numbers are commonly given to fabrics reflecting high driving force (high supersaturation), which result in spherulitic growth. These are absent in Mairs stalagmites, which are dominated by columnar calcite. Thus, the progression of numbers in the fabric stratigraphy (log) reflect an increasing amount of impurities "polluting" clean columnar calcite (1), which result in the development of faint laminae (2), parallel and visible laminae (3), laminae with triangular-shaped (rhombohedra) tips (4) up to the point when from compact the fabric becomes open (5). Then, the criteria follow a similar *r* pattern (open columnar with faint laminae, 6; with parallel visible laminae, 7; with rhombohedra tips, 8). Eventually, impurities coat the stalagmite top, crystals cease to grow in optical continuity with the substrate, and re-nucleation occurs (number 9). The resulting microstratigraphy eventuated by the fabric logs for MC-S1 and MC-S2 were tied to the stable isotope and age measurement slabs by comparing high-resolution scans of both thin sections and polished slabs.

The Al and U concentration data (not shown) were used as a broad guide to select calcite with low-detrital and highest U content for age measurements. Both stalagmites were examined in thin section. Fabric and possible dislocations in growth were documented and also used to guide subsampling for age measurements. U-Th age measurements were conducted at the University of Melbourne following the methods of Hellstrom (2003; Table 1). Briefly, samples of 20–120 mg were dissolved in concentrated HNO_3 and equilibrated with a mixed ^{229}Th–^{233}U tracer. U and Th were extracted in a single solution using Eichrom TRU resin before introduction to a Nu Plasma multi-collector ICPMS, where isotope ratios of both elements were measured simultaneously. Initial [^{230}Th / ^{232}Th] was defined via modelling the age and depth data for MC-S2 and determined to be 0.58 ± 0.29. The uncertainty was fully propagated for both stalagmite age models using Monte Carlo simulations of Eq. (1) in Hellstrom (2006). The method for the age–depth model is described in Hendy et al. (2012) and Scholz et al. (2012). The decay constants of Cheng et al. (2013) were used. Detrital content is low for MC-S1 resulting in negligible corrections of < 0.4 %. Corrections for MC-S2 were variable (0.1–5.4 %) depending on proximity to sediment layers. Nine of the 19 ages used to construct the Mairs Cave chronology appeared in Cohen et al. (2011) and are updated in Table 1 for completeness.

Table 1. U and Th isotope data and age determinations (in depth order) for stalagmites MC-S1 and MC-S2, Mairs Cave, Flinders Ranges, South Australia. Square brackets indicate activity ratios. MCS2-UM10 was omitted from the age–depth model as it is out of stratigraphic order.

Sample ID (lab no.)[a]	Depth (mm)[b]	U ($ng\,g^{-1}$)	$[^{230}Th/^{232}Th]$	$[^{230}Th/^{238}U]$[c]	$[^{234}U/^{238}U]$	Uncorr. age (ka)	Corr. age (ka)[d]	Corr. initial $[^{234}U/^{238}U]$
MCS1-UM7(A01962)*	1.0[1.0]	121	1986	0.3766(16)	2.8639(47)	15.15(0.07)	15.15(0.07)	2.9453(47)
MCS1-UM8(A01963)*	2.9[1.6]	133	907	0.3826(10)	2.8358(52)	15.57(0.05)	15.56(0.05)	2.9182(53)
MCS1-UM3(A01573)*	7.5[0.4]	115	1189	0.3666(13)	2.6761(55)	15.83(0.07)	15.82(0.07)	2.7526(56)
MCS1-UM4(A01574)*	32.7[0.4]	115	1271	0.3360(15)	2.3991(48)	16.22(0.08)	16.22(0.09)	2.4646(49)
MCS1-UM5(A01575)*	77.6[0.8]	140	2175	0.3295(14)	2.2842(41)	16.75(0.08)	16.75(0.08)	2.3463(42)
MCS1-UM6(A01576)*	104.5[1.0]	117	1366	0.3512(15)	2.3819(49)	17.14(0.09)	17.13(0.09)	2.4503(51)
MCS2-UM1(A02109)*	2.1[1.5]	74	189	0.2455(26)	1.7728(37)	16.08(0.19)	16.04(0.19)	1.8086(38)
MCS2-UM11(D120907-256)	7.8[1.5]	95	43	0.2554(18)	1.6656(48)	17.96(0.15)	17.73(0.18)	1.6997(50)
MCS2-UM07(B04007)	8.5[1.0]		15	0.2629(52)	1.6708(66)	18.46(0.40)	17.82(0.51)	1.7054(70)
MCS2-UM08(B03992)	11.0[1.7]		54	0.2536(57)	1.6385(94)	18.14(0.45)	17.97(0.47)	1.6717(97)
MCS2-UM4(A02778)*	18.9[1.5]	172	793	0.2601(16)	1.6157(28)	18.93(0.13)	18.92(0.13)	1.6495(29)
MCS2-UM10(B03993)	21.3[0.8]		58	0.2586(48)	1.6502(100)	18.381(0.39)	18.22(0.40)	1.6845(105)
MCS2-UM12(D120907-260)	22.5[1.0]	81	111	0.2707(22)	1.6748(57)	19.00(0.18)	18.91(0.19)	1.7118(59)
MCS2-UM05(B03826)	39.5[2.0]	225	636	0.2812(18)	1.6162(34)	20.60(0.15)	20.58(0.15)	1.6530(35)
MCS2-UM2(A02110)*	44.3[1.5]	151	27	0.2959(16)	1.6604(30)	21.13(0.13)	20.72(0.25)	1.7002(31)
MCS2-UM13(D120907-271)	64.5[1.5]	206	46	0.2987(16)	1.5746(46)	22.65(0.15)	22.39(0.20)	1.6121(48)
MCS2-UM06(B03829)	76.4[1.3]	332	10	0.3177(21)	1.5688(33)	24.34(0.19)	23.02(0.68)	1.6070(36)
MCS2-UM14(D120907-312)	77.5[1.0]	230	19	0.3098(18)	1.5633(44)	23.77(0.17)	23.12(0.37)	1.6013(46)
MCS2-UM15(D120907-404)	94.8[1.5]	273	22	0.3128(16)	1.5203(43)	24.79(0.16)	24.22(0.33)	1.5571(45)

[a] Asterisked samples appear in Cohen et al. (2011). Prefix for lab analysis number is "UM".
[b] Median depth from top. Square brackets indicate thickness of calcite wafer.
[c] Figures in brackets are 2σ uncertainties of the least significant digits.
[d] Age correction is based on $[^{230}Th/^{232}Th]_{initial} = 0.58 \pm 0.29$; and decay constants given in Cheng et al. (2013).

4 Results

4.1 Speleothem chronology

The Mairs Cave speleothem record presented here is dated by a total of 19 high-precision U-series disequilibrium age measurements (Table 1; Fig. 2a, b; age–depth plots are given in Fig. S1 of the Supplement) and collectively spans 24 to 15 ka. A lens of calcite formed at the base of MC-S2 at 24.2 ka that was subsequently covered by sediment, before calcite recommenced growing at 23 ka. The exact growth interval of this lower lens could not be constrained with further age measurements owing to the amount of detrital material in this section. Age modelling shows that MC-S2 grew relatively slowly at $10\,\mu m\,a^{-1}$ (Fig. 3b). Taking into account potential additional accretion by sediment layers in this section (Fig. 2b) suggests growth may have been slower or possibly episodic, although age measurements made immediately either side of crystal growth dislocations identified in thin section were found to be within error of each other, suggesting that any suspension of growth was not for any significant duration. On these grounds, the short-lived peaks in growth rate at 19 and 20.6 ka (Fig. 3b) are artefacts produced by the age model on closely spaced age measurements. MC-S2 growth slowed to $3\,\mu m\,a^{-1}$ at 17.7 ka until growth terminated at $15.6 + 0.6/-1.6$ ka, based on extrapolation of the 3rd and 97th percentile of the age–depth model to the top of the speleothem. This uncertainty largely reflects the slow growth rate through this section.

MC-S1 growth was initiated by 17.2 ka at a moderate rate ($60–90\,\mu m\,a^{-1}$) until 15.8 ka, when growth decreased 10-fold until it terminated at 14.9 ka (Fig. 3b). It should be noted that the beginning of this phase may have begun earlier (i.e. approximately 17.6 ka extrapolated from growth rate) as the very oldest portion of MC-S1 was not able to be sampled (Sect. 3.1). Overall, MC-S1 grew approximately 10 times faster than MC-S2.

4.2 Calcite fabric in thin sections

Both stalagmites are comprised predominately of columnar calcite. The compact columnar fabric of MC-S2 is, in its lower part (pre-20.6 ka), punctuated by several (> 20) thin detrital layers, most evident on the vertical flank of the stalagmite (Fig. 3c). Calcite re-nucleation occurs above the detritus rich layer and is marked by geometric selection whereby only crystals best aligned for mass-transfer processes within the environment of deposition continue to grow at the expense of neighbouring crystals (see Gonzalez et al., 1992; Self and Hill, 2003). However, growth of the dominant forms mostly occurred in optical continuity with the substrate. In the upper 40 mm (post-20.6 ka) the sediment layers cease to drape over the growth axis although sediment lenses are still evident on the flank of the stalagmite up until ca. 18.9 ka (Fig. 2b). In this portion of the stalagmite, the fabric is compact columnar calcite and lamination is not visible or extremely faint (Fig. 3c).

By comparison, MC-S1 fabric is characterised by both compact, translucent and open, milky columnar subtypes

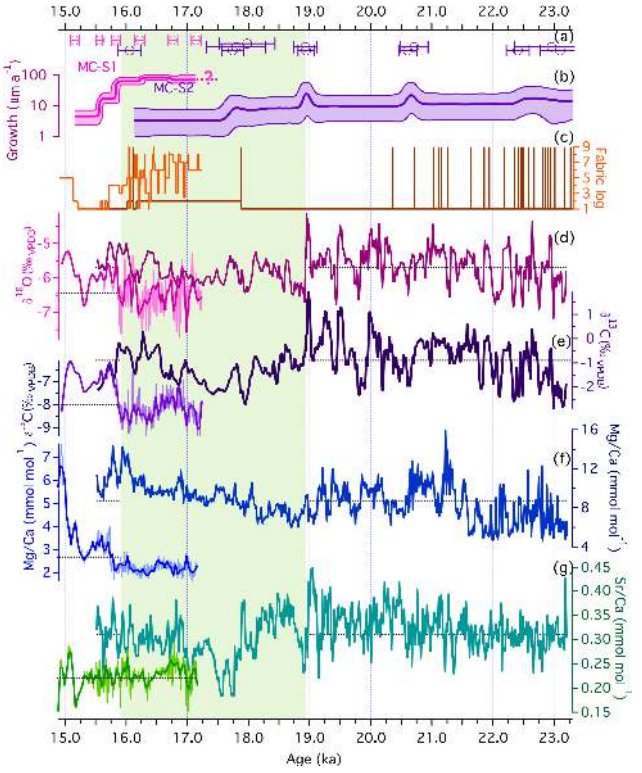

Figure 3. Mairs Cave stalagmites MC-S1 and MC-S2: age measurements **(a)**, growth rate **(b)**, fabric log **(c)**, δ^{18}O **(d)**, δ^{13}C **(e)**, Mg / Ca **(f)**, and Sr / Ca **(g)**. Note different offset scales on left and right-hand axes for panels **(e)** to **(g)**. Short-lived peaks in growth rate at 19 and 20.6 ka are artefacts of closely spaced age measurements. Fabric log indicates calcite fabric classification, where values 1 to 8 indicate a scale, ranging as follows: closed columnar without laminations (1), columnar with faint laminations, parallel laminations and rhombohedral tips (2 to 4), open columnar calcite (5), and open columnar with faint laminations, parallel laminations and rhombohedral tips (= 6 to 8); "9" marks re-nucleation episodes with geometric selection and possible dissolution. The hierarchy scale suggests increasing discharge and impurities content. Fine dotted line in panels **(d)** to **(g)** are mean values for each stalagmite. Pale green shading indicates an inferred relatively wetter phase.

with well-defined laminae. The laminae are particularly well defined by the presence of brown organic-rich calcite from the base to 6 mm below the top (i.e. 17.2–15.6 ka; Fig. 3c). The fabrics were further defined by the shape of the crystal tips, which were flat or acute (Turgeon and Lundberg, 2001; Frisia, 2015). Such distinction allows an immediate recognition of the original thickness of the film of fluid bathing the stalagmite tip (Turgeon and Lundberg, 2001). Mairs cave columnar fabrics are characterised by two common types of crystal terminations as seen in thin section: rhombohedra (which appear as a triangle) and flat (which appear as a line). The rhombohedra tips reflect the emergence of either cleavage {10.1}, steep {01.2}, or acute {40.1} rhombohedra at the speleothem surface at the time of formation. Of these, the {10.1} and {40.1} are the most commonly observed forms in speleothems, as the steep rhombohedron is more typical of marine waters, at higher supersaturation than the typical cave waters. The steep form also yields length-fast individuals (see Fairchild and Baker, 2012), which is not the case of MC-S1 and MC-S2 columnar crystals. The height of the rhombohedra "tips" in both stalagmites suggest that they grew in a film of fluid of up to 100 µm (Fig. 2c). Flat terminations can be interpreted as the result of growth from a very thin, less than 20 µm, film of fluid. However, oxidation of organic matter due to microbial activity when growth is intermittent (or absent) could potentially lead to partial dissolution of the underlying calcite crystal tips, which results in their "flattened" appearance (see Fairchild and Baker, 2012). As small dissolutional features are associated with both rhombohedra and flat terminations of crystals below dark layer in laminae (Fig. 2c) then it is reasonable to assume that drip rate was the primary control on the formation of these laminae in MC-S1, with rhombohedra tips indicative of higher drip rate and flat tips of relatively dry periods. Typically, these laminae group in bundles with flat or rhombohedral tips (Fig. 3c). The thickness of the bundles ranges from approximately 400 to 1200 µm. Within these bundles, laminae are approximately 20–100 µm thick (Fig. 2c), suggesting that they may be subannual to annual features, judged against the mean growth rate of MC-S1 through this section, although their thickness is erratic with time.

4.3 Mairs Cave speleothem records

4.3.1 Speleothem δ^{18}O

MC-S1 and MC-S2 δ^{18}O data spanning 23.2–14.9 ka are shown in Fig. 3d. Considering the longer MC-S2 record, mean δ^{18}O is 0.3 ‰ lower than the long-term mean (−5.7 ‰) during 23.2–22.0 ka and close to the mean from 22–18.9 ka (Fig. 3d). In the interval of 23.2–18.9 ka, the δ^{18}O record contains multi-decadal to centennial variability of up to 2.5 ‰ that dominates over longer-term variability (Fig. 3d). This shorter-term variability is characterised by rapid transitions to isotopic minima that are relatively short-lived (typically 20–70 years), separated by longer intervals (50–200 years) of higher values, often displaying a rising trend, i.e. forming a saw-tooth type pattern. Post-18.9 ka, MC-S2 δ^{18}O is 0.2 ‰ lower than the mean until ∼ 16.5 ka, during which the shorter-term variability is relatively dampened. This is not an artefact of sampling resolution as MC-S2 growth rate through this transition is constant (Fig. 3b). Afterwards, δ^{18}O rises above the mean by 0.2 ‰ overall, until MC-S2 growth ceases at 15.6 ka.

The shorter duration but faster growing MC-S1 record is approximately 0.5 ‰ lower compared with MC-S2 during the overlapping growth period (17.2–15.6 ka) during which MC-S1 is dominated by decadal isotopic variability of 1–1.5 ‰ (Fig. 3d). To compare the records more closely, a

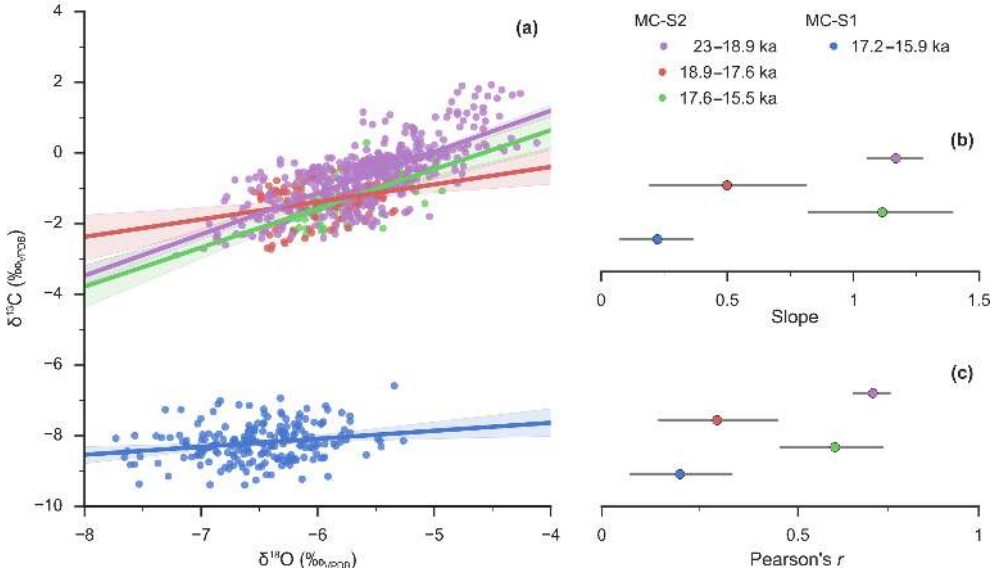

Figure 4. Scatter plot of MC-S1 and MC-S2 δ^{18}O and δ^{13}C data for key intervals in the record **(a)**, slopes **(b)**, and r values **(c)** for these same intervals. Higher slope and r values indicate relatively higher isotopic disequilibrium.

smoothing spline was applied to MC-S1 δ^{18}O data reducing its resolution over the common growth interval with MC-S2 by a factor of 4. MC-S1 contains millennial-scale oscillations of approximately 1 ‰, defined by relatively short-lived minima. MC-S2 also contains similar features but a close comparison is hampered by the relatively poorer precision of the MC-S2 chronology over this interval. At 15.8 ka, MC-S1 δ^{18}O rises 1 ‰ coinciding with the 10-fold decrease in growth rate (Fig. 3b, d). Post-15.8 ka, MC-S1 δ^{18}O is 0.5 ‰ higher than the overall mean apart from a brief trough at 15.3 ka. MC-S1 terminates at 14.9 ka with a relatively high δ^{18}O value of −5.3 ‰.

4.3.2 Speleothem δ^{13}C and its relationship with δ^{18}O

Mean MC-S2 δ^{13}C is particularly high (−0.9 ‰), being 7.1 ‰ more enriched than MC-S1 overall (Fig. 3e). Prior to 18.9 ka, there are broad similarities with the δ^{18}O record, with MC-S2 δ^{13}C typically lower than the long-term mean until 22 ka and typically higher from 22 to 18.9 ka (Fig. 3e). MC-S2 δ^{13}C is also characterised by multi-decadal to centennial variability that is equivalent to or larger in magnitude (1–2 ‰) than millennial trends. In almost all cases, prominent δ^{18}O minima coincide with δ^{13}C minima but the relationship between the two isotopes appears to weaken between troughs. Maxima occasionally exceed 0 ‰ (δ^{13}C) particularly between 20 and 18.9 ka (Fig. 3e). Trends in MC-S2 δ^{13}C depart from δ^{18}O after 18.9 ka, with δ^{13}C declining approximately 2 ‰ until 17.7 ka, before rising again towards the termination of this record.

With respect to millennial trends, MC-S1 δ^{13}C rises from 17.2 to 16.8 ka, coinciding with rising values in MC-S2, but returns to lower values between 16.4 and 15.8 ka (Fig. 3e). MC-S1 δ^{13}C sharply rises by 2.5 ‰ at 15.8 ka, typically remaining high during this period of slow growth, apart from the reversal that also coincides with the δ^{18}O trough at 15.3 ka. Similar to the δ^{18}O record, MC-S1 δ^{13}C is characterised by multi-decadal isotopic variability of approximately 1 ‰, i.e. similar or lower in magnitude versus δ^{18}O. As for the MC-S2 record, troughs in both isotopes coincide with regard to timing.

Scatter plots (Fig. 4a) show that MC-S2 δ^{18}O and δ^{13}C are moderately correlated during the earlier growth phase of 23.2–18.9 ka ($r = 0.7$, slope 1.2), weaker during 18.9–17.6 ka ($r = 0.3$, slope 0.5), and moderately correlated again during 17.6–15.5 ka ($r = 0.6$, slope 1.2) (Fig. 4b, c). A correlation between δ^{18}O and δ^{13}C may indicate isotopic disequilibrium at the time of speleothem deposition (Hendy and Wilson, 1968). We note that MC-S2 shows no isotopic enrichment between axial and off-axis transects (13 mm apart; Fig. S1), in either of the growth phases 23.2–18.9 or 17.6–15.5 ka, suggesting that calcite precipitation across the top of the stalagmite growth is occurring close to isotopic equilibrium. We note also that the high-frequency isotopic variability is often as large, or larger, in magnitude for δ^{18}O as for δ^{13}C. Typically, kinetic effects result in C isotopic enrichment dominating O by about a factor of 2–4 (Fantidis and Ehhalt, 1970; Hendy, 1971; Mickler et al., 2006).

4.3.3 Spectral analysis of short-term δ^{18}O variability

A notable characteristic present in each of the speleothem isotopic records is the coincident troughs in both isotopes defining a saw-tooth pattern, particularly in regard to δ^{18}O.

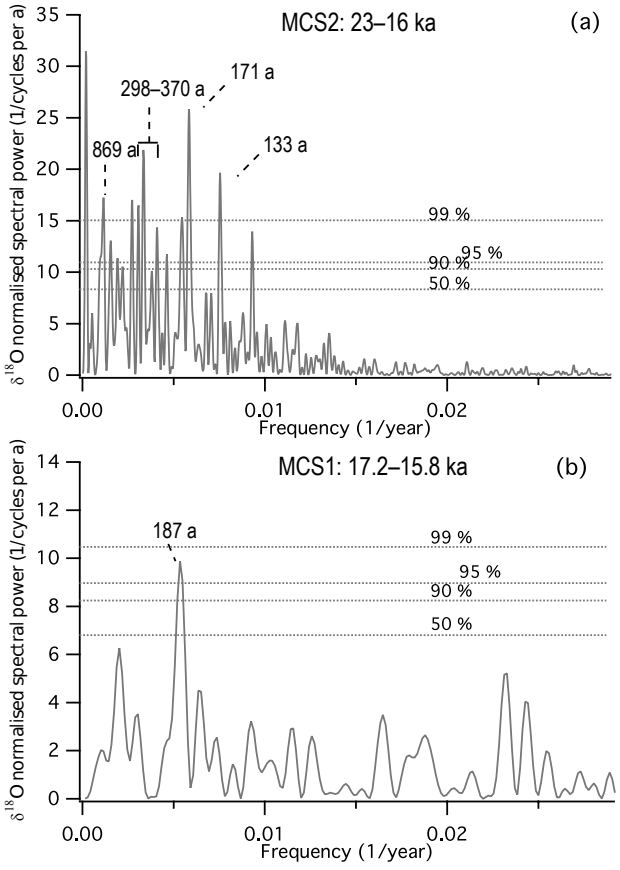

Figure 5. Spectral analysis of MC-S1 and MC-S2 δ^{18}O between 23.0–15.8 ka using the Lomb–Scargle method (Press and Rybicki, 1989). Horizontal dotted lines indicate confidence intervals.

The magnitude of these transitions can be up to several per mil with regard to δ^{18}O or δ^{13}C and is isotopically larger than millennial trends. Spectral analysis was conducted on MC-S1 (17.2–15.8 ka; post-15.8 ka was excluded due to low resolution of these data) and MC-S2 (23.0–16.0 ka) δ^{18}O records (Fig. 5a, b). The sole statistically significant peak in MC-S1, at 187 ± 15 years, is also present and significant in MC-S2 at 171 ± 15 years. The uncertainty in the spectral peak locations was estimated by propagating the 2σ error of age measurements at the ends of each record. MC-S2 exhibits a richer spectrum, with periods that are multiples of ~ 180, including one near 360 years which is perhaps the fundamental period of the ~ 180 year peak, as well as an additional periodicity at $\sim 133 \pm 15$ years. The 180 ± 15-year cycles persist through the 18.9 ka transition in the record, verified by repeating the spectral analysis on segments either side of 18.9 ka (not shown).

4.3.4 Mairs Cave speleothem Mg / Ca and Sr / Ca

Speleothem mean Mg / Ca and Sr / Ca ratios are higher in MC-S2 versus MC-S1 (Mg / Ca: 9.5 vs. 2.7 mmol mol^{-1}; Sr / Ca: 0.29 vs. 0.23 mmol mol^{-1}; Fig. 3f–g). There are similarities with the isotopic record, namely lower ratios prior to 22 ka, a decrease in ratios at 18.9 ka, and higher ratios towards the termination of the records from 16.0 to 15.8 ka onwards. The last observation is clearest in the case of Mg / Ca, where ratios become 50–200 % higher. MC-S2 Mg / Ca contains a rising trend that coincides with rising δ^{13}C from 18 ka onwards.

MC-S2 Mg / Ca also contains decadal to centennial variability that is more prominent prior to 18.9 ka, but these features are less clear than the saw-tooth pattern observed in the isotopic record (Fig. 3d–e). These features are almost entirely absent in the MC-S1 Mg / Ca record (Fig. 3f), suggesting that the multi-decadal to centennial isotopic variability cannot fully be a product of post-infiltration karst processes.

With regard to Sr / Ca, there is better agreement between speleothem records in terms of mean Sr / Ca values (15 % offset vs. 72 % offset for Mg / Ca) and possibly also centennial–millennial trends. There are higher Sr / Ca values in both speleothems 17.0–16.6 ka, coinciding with higher δ^{13}C, and prominent shorter-lived maxima from 16 ka onwards appearing in both speleothems, but the chronological uncertainty in MC-S2 prevents direct correlation. Post-18.9 ka, Sr / Ca also declines to a minimum at 17.5–17.7 ka coinciding with a minimum in δ^{13}C.

The relationship between speleothem Mg / Ca and Sr / Ca can be used to diagnose prior calcite precipitation (PCP). PCP is the calcite that precipitates from the parent water before it reaches the stalagmite (Fairchild and Baker, 2012). According to a theoretical derivation, the slope of ln(Mg / Ca) vs. ln(Sr / Ca) should equal 0.88 ± 0.13 if PCP is dominating (Sinclair et al., 2012). In these datasets, calculated slopes were close to zero, as there were no consistent relationships between these two variables in either speleothem ($r = 0$ to -0.1 over all key periods of interest; Supplement Fig. S2). This suggests that PCP is not dominating one or either of these elements. To investigate this further, we calculated the predicted variation in Mg / Ca, due to PCP, based on Sr / Ca variability. From Sinclair et al. (2012), if PCP is dominating both elements, then $\Delta\ln(\mathrm{Sr}/\mathrm{Ca}) / \Delta\ln(\mathrm{Mg}/\mathrm{Ca}) = 0.88$ (weight ratio). One SD of our ln(Sr / Ca) data is 0.16; thus, the equivalent predicted variability in ln(Mg / Ca) would be just 0.18, which is approximately 13 times smaller (in mmol mol^{-1} units) compared with 1 SD of our measured ln(Mg / Ca) values (0.47). Similarly for MC-S1, the measured variability is 10 times greater than predicted by the PCP relationship. Hence, these calculations suggest that some other process is dominating any potential PCP signal in our data, and that this process has a greater impact on our Mg / Ca versus our Sr / Ca signal. This suggests that the Mg / Ca signal is complex at this site,

consistent with the likelihood that Mg has multiple sources. This is consistent with other karst studies in Australia in water-limited regions where there are a greater number of identified sources and modifying processes for Mg (sea salt, dust, clay sorption, bedrock, biomass) compared to Sr, which has been found to be dominated by bedrock and dust alone (e.g. Goede et al., 1998; Rutlidge et al., 2014; Treble et al., 2016).

Further detailed comparison with the isotopic record was attempted to tease out potential drivers such as soil processes, dilution, and autochthonous versus allochthonous sources. For example, lowered Mg / Ca coinciding with declining δ^{13}C and lower δ^{18}O from 19 to 18 ka could indicate a declining aeolian source during a period of soil stabilisation. The decline in aeolian contribution is also suggested by the progressive decrease in the detrital and re-nucleation layers from 23.0 to 20.6 ka and their disappearance after 18.9 ka, i.e. a reduction in supply. Further detailed analyses, probably requiring a larger suite of trace elements, may be carried out in a future study to fully investigate this. In this present study, we simply draw from the broad similarities between Mg / Ca, Sr / Ca, and the isotopic record for (i) the multi-decadal to centennial-scale variability prior to 18.9 ka, (ii) the transition at 18.9 ka, and (iii) the rise in these signals after 15.8 ka, to argue that these features are broadly hydrologically driven.

5 Discussion

5.1 Mairs Cave stalagmites as a record of groundwater recharge

5.1.1 Isotopic disequilibrium as an indicator of recharge during 23.0–18.9 ka

There are several characteristics that suggest that isotopic disequilibrium is impacting the Mairs Cave speleothem record and that this impact varies through time and spatially between stalagmites: (i) MC-S2 is isotopically enriched compared with MC-S1, (ii) relatively slow growing MC-S2 has particularly high mean δ^{13}C overall (−0.9 ‰), and (iii) δ^{18}O and δ^{13}C are moderately correlated during the earlier growth phase 23–18.9 ka ($r = 0.7$).

Typically, isotopic disequilibrium is considered to be caused by either (i) fractionation during the degassing process enhanced by high dripwater supersaturation and slow drip rates (Fantidis and Ehhalt, 1970; Day and Henderson, 2011) or (ii) fractionation driven by within-cave evaporation, from either low relative humidity or high ventilation (Deininger et al., 2012). We can expect several of these to be more common in semi-arid karst settings (e.g. low drip rates, low cave air relative humidity; Cuthbert et al., 2014a). However, it appears that the calcite has precipitated closer to isotopic equilibrium across the top of stalagmite MC-S2 (Sect. 4.3.2). This suggests isotopic disequilibrium could be occurring in the parent dripwaters, perhaps by incomplete equilibration or evaporation in the soil/epikarst karst stores (Bar-Matthews et al., 1996; Cuthbert et al., 2014a). The fact that variability in δ^{18}O is as large or larger than for δ^{13}C (Sect. 4.3.2) supports the argument that considerable evaporation of the soil/epikarst waters occurred.

We argue that the impact of recharge is also evident in the multi-decadal to centennial variability, which appear as saw-tooth type features displaying rapid 1–2.5 ‰ decreases in δ^{18}O, separated by longer periods of ^{18}O enrichment, often reaching a maxima immediately before an abrupt transition into a trough. The δ^{18}O minima typically coincide with δ^{13}C troughs, and occur throughout a period of relatively elevated mean δ^{13}C (Fig. 3d, e). This is consistent with a model of infiltration-driven disequilibrium effects in a semi-arid karst environment, with (i) δ^{18}O minima representing times of recharge when dripwater is least fractionated by evaporation in the soil/vadose zone and/or in the cave (as recharge stimulates faster dripping), and (ii) δ^{13}C minima are related to increased soil CO_2 bioproductivity and/or less fractionation. The δ^{18}O variation is consistent with isotopic modification of dripwaters of up to 2 ‰ observed during monitoring of a modern semi-arid environment at Wellington Caves (Cuthbert et al., 2014a).

The persistence of sediment bands representing cave floor flooding, the erratic thickness of MC-S1 laminae argued to be drip-rate-controlled, and the occasional dissolution feature identified via thin section further support a hydrological driver, i.e. that the cave is affected by intermittent recharge. Dissolution features in this time interval implicate occasional rapid infiltration of high intensity events resulting in soil zone bypass or inundation by floodwaters.

5.1.2 Recharge during the LGM

The abrupt shift in the isotopic records at 18.9 ka, coinciding with the peak of the LGM, is characterised by (i) a 2 ‰ abrupt decrease in both δ^{18}O and δ^{13}C, (ii) reduced isotopic amplitude, and (iii) weak co-variation between δ^{18}O and δ^{13}C, which persists for at least several millennia (Fig. 3d, e). Based on the above proposed infiltration/disequilibrium model, the isotopic data suggest a shift in hydrological regime to more effective recharge and/or reduced evapotranspiration from 18.9 until 15.8 ka. The dampening of the δ^{18}O signal suggests enhanced storage of dripwater aided by relatively greater recharge. Enhanced recharge is also supported by the coincident reduction in Mg / Ca ratios (Fairchild and Treble, 2009; Tremaine and Froelich, 2013; Belli et al., 2017).

The absence of sediment bands in MC-S2 after 18.9 ka (Fig. 2b) could also suggest a hydrological change, although we cannot exclude that this is simply a function of the stalagmite growth outpacing streamwater levels or a reduction in sediment supply. MC-S1 began growing by 17.2 ka during this proposed period of enhanced recharge. Initiation of a new stalagmite suggests activation of a new flow path, further

supporting more effective recharge. The occurrence of bundles of laminae showing parallel versus rhombohedra-tipped layers suggests that the increase in effective recharge varied, periodically, from 17.2 to 16.2 ka (Fig. 3c), with episodes of dissolution (highest recharge of undersaturated waters) between 16.7 and 16.2 ka. The presence of laminae indicates input of colloidal particles during infiltration when water was at its lowest supersaturation state (Frisia et al., 2003). The occurrence itself of the visible organic colloids would suggest that maximum infiltration occurred in a cooler context (Frisia et al., 2003), which prevented efficient organic matter degradation.

Our spectral analysis demonstrates that multi-decadal to centennial variability in speleothem δ^{18}O persists through the LGM and early deglaciation. Speleothem δ^{18}O can be related to rainfall characteristics such as rainfall amount, moisture source, and/or trajectory effects, and this has been examined in the modern record for southwest Australia, located at similar latitudes to Mairs Cave (Treble et al., 2005; Fischer and Treble, 2008). It may be tempting to interpret this multi-decadal variability in the Mairs Cave δ^{18}O record as being directly related to rainfall isotopic variability such as our 1974 modern analogue (Sect. 2), during which particularly low rainfall isotopic values were recorded in Adelaide (-10 ‰ compared with precipitation-weighted annual mean of -4.5 ‰; IAEA/WMO, 2006) owing to the "continental effect" (Welker, 2000).

However, we consider that, in a semi-arid environment, moisture source variation cannot be reliably fingerprinted owing to the additional isotopic impact of evaporation of water in karst stores between recharge events (Cuthbert et al., 2014a, b), as well as the likely scenario that recharge will be biased to intense δ^{18}O low rainfall events in order to overcome non-linear karst recharge thresholds in environments such as these (Markowska et al., 2016). Thus, while the δ^{18}O minima that occur throughout the Mairs Cave record are related to recharge, and the overall isotopic variability to water balance, the magnitude of these minima cannot be judged as an isotopic fingerprint, i.e. tropical versus mid-latitude derived moisture, as in this environment the isotopic relationship between climate and the resulting speleothem record will be exaggerated by infiltration and post-infiltration processes.

A final point to raise when considering mean speleothem δ^{18}O during the LGM is that cave temperature and ice volume would also have had an impact on these values. We modelled this following Griffiths et al. (2009) (Supplement Fig. S4). This modelling suggested that these effects could account for +2 ‰ of the δ^{18}O signal at 18.9 ka relative to 16 ka. However, such a figure is probably a maximum and cannot realistically be constrained, as other factors impact precipitation δ^{18}O. For example, a cooler LGM atmosphere would counteract isotopic depletion, as well as the isotopic impact of evapotranspiration and atmospheric source/trajectory effects. We note the fact that millennial variation is isotopically smaller than the decadal–centennial variation suggests that it does not exceed the hydrological uncertainty in the Mairs Cave speleothem isotopic record.

5.1.3 Shift to aridity at 15.8 ka

The point 15.8 ka marks a transition in the Mairs Cave record evidenced by an abrupt +1 ‰ step shift in MC-S1 δ^{18}O and +2.5 ‰ in δ^{13}C (Fig. 3d, e). This is accompanied by higher Mg / Ca values, an almost 10-fold reduction in growth rate, and the shift towards closed columnar fabric without lamination (Fig. 3b–c, f). From 15.8 ka (Fig. 3c) the columnar calcite is fully closed (1 on fabric log) and laminae are either absent or faint. This suggests that there was less input of colloidal organic matter from the soil zone. Furthermore, clean, compact columnar calcite in well-monitored caves of temperate alpine settings, has been documented to form at low supersaturation (Frisia et al., 2000; Borsato et al., 2015, 2016) and temperatures ranging from 13.2 to 9.2 °C (Borsato et al., 2015). By contrast, open columnar formation is enhanced when temperature drops (in the range 9.2 to 4.2 °C) if supersaturation remains low, as impurities are more effective in blocking growth sites. Thus, it is reasonable to infer that Mairs Cave stalagmite fabrics reflect both a change in hydrology and an increase in temperature from 15.8 ka until growth ceased.

The transition in the MC-S1 record at 15.8 ka also occurs approximately at the time of overall isotopic enrichment and higher Mg / Ca in the MC-S2 record, followed by termination of MC-S2 growth (given the chronological uncertainty; Fig. 3a, d–f). The response of these variables is consistent with a drying signal. A similar response was observed during a multi-decadal drought period recorded in a modern speleothem in the southern Australian region (Treble et al., 2005) and elsewhere (Asrat et al., 2007). The shift to aridity at 15.8 ka in the Mairs Cave record is a particularly robust signal given the multiple lines of evidence, i.e. termination of MC-S2 and the abrupt shift in hydrologically sensitive proxies in MC-S1. Termination of MC-S1 at (~ 14.9 ka) is consistent with the impact of persistent drying, possibly resulting from depletion or loss of connectivity with the shallow vadose water store feeding MC-S1.

5.2 Comparison of Mairs Cave record with other archives

5.2.1 Regional geomorphology records

The Mairs Cave record overlaps chronologically with a nearby sedimentary archive, the "Flinders silts" (Fig. 1b), a thick sequence (up to 18 m) of slackwater laminae from the western side of the central Flinders Ranges (Callen, 1984; Haberlah et al., 2010). These fluvial deposits are approximately 100 km from Mairs Cave and date from ~ 24 to ~ 16 ka and consist of fine-grained silts, originally blown from a deflated Lake Torrens to the west (Fig. 1b), but were

fluvially re-worked and deposited by back-flooding of narrow gorges from 47 until 16 ka (Haberlah et al., 2010). Laminae are interpreted to represent rapid deposition from floods with approximately centennial frequency during 24–19 ka, with storms interpreted to have reduced in frequency and/or magnitude after 19 ka, and termination of flood laminae at 16 ka.

The Mairs Cave and Flinders silts records correlate remarkably well in terms of their timing of hydrological change with a "switching-on" of recharge at 24 ka and "switching-off" at 16 ka and a significant change in the hydrological characteristics at 19 ka. However, they differ somewhat in the interpretation of the hydrological change at 19 ka, i.e. reduced storm frequency/intensity in the silt record versus more effective recharge in the stalagmite record. Although speculative, combining this evidence may indicate something of the nature of this change in terms of the frequency/magnitude characteristics of the rainfall, i.e. a shift to more frequent, lower-magnitude events leading to more continuous recharge, or the speleothem isotopic record may just reflect reduced evapotranspiration over this interval. The records do agree in the 23–19 ka interval in terms of significant hydrological events of approximate centennial frequency, i.e. high-magnitude floods in the silts record are consistent with significant recharge occurring approximately every 130–180 years in the Mairs Cave record.

We note here, also, that it was previously unresolved whether the termination of Flinders silts at 16 ka was due to a lack of floods or the exhaustion of silt supply (Haberlah et al., 2010). However, the match with the abrupt transition to aridity in our data supports a climatic driver for the termination of the floodwater lamina.

Increased hydrologically effective precipitation in the 19–16 ka period is also supported by optically stimulated luminescence ages from beach ridges at Lake Frome (Fig. 1a), indicating that it was 15–20 times the modern volume between 18 and 16 ka (Cohen et al., 2011, 2012), coincident with relatively high levels of charcoal and woodland taxa pollen present in the sediments of the lake floor (Singh and Luly, 1991; Luly, 2001). The shift to aridity at 15.8 ka in Mairs Cave is supported by significant reductions in *Callitris* sp. pollen and charcoal (Singh and Luly, 1991). Fluvial records for the Goulburn, Lachlan and Gwydir catchments also indicate a wetter LGM interval, although the timing is either variable between catchments or lacks precision (Bowler, 1978; Kemp and Rhodes, 2010; Pietsch et al., 2013). The Strzelecki dune fields to the north and east of the Flinders Ranges (Fig. 1a) record an interval of pedogenesis (indicating relative stability) from ~ 19 ka, followed by a major phase of dune reactivation ~ 15–14 ka (Fitzsimmons et al., 2009). Evidence for a high lake phase at Lake Mungo (Fig. 1a) (Willandra Lakes system) was also recently reported but dated to 24 ka (Fitzsimmons et al., 2015).

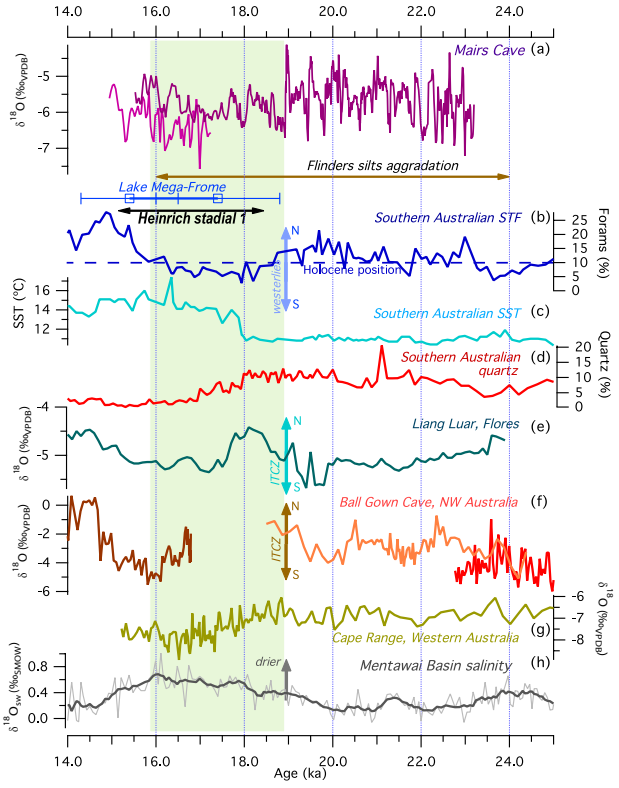

Figure 6. The Mairs Cave $\delta^{18}O$ record **(a)** compared with the foraminifera record **(b, c)** and the quartz record **(d)** in marine core MD03-2611 from the Murray Canyons region, southern Australia (De Deckker et al., 2012). Speleothem records from Liang Luar, Flores (Ayliffe et al., 2013) **(e)**; Ball Gown Cave, Western Australia (Denniston et al., 2013a) **(f)**; and C126 Cave in Cape Range, also in Western Australia (Denniston et al., 2013b) **(g)**. Reconstructed salinity from marine care SO189-39KL from the northern Mentawai Basin, Indonesia **(h)**.

5.2.2 Comparing Mairs Cave with the MD03-2611 marine record

Comparing the Mairs Cave record with the MD03-2611 marine record (De Deckker et al., 2012) reveals that the transitions identified in the STF record also coincide remarkably with those at Mairs Cave in terms of timing, i.e. 19 and 16 ka (Fig. 6b). However, we highlight the following inconsistency. The MD03-2611 STF record is interpreted as a proxy of westerly winds, with the westerlies interpreted to have shifted *further* from Australia between 19 and 16 ka. This implies a *reduction* in moisture from the westerlies during the same interval during which we interpret an *increase* in recharge to the Flinders Ranges. Further to this, at 16 ka, the marine record indicates that the westerlies have shifted closer to Australia and even further *north* of their Holocene location, implying restored westerly airflow over southern Australia, at the same time that we observe a shift to aridity. The MD03-2611 quartz record, interpreted as an indicator of

aeolian activity over southern Australia, implies a reduction in aridity after 18 ka. This is somewhat consistent with the Mairs Cave record, although nearly 1000 years later in terms of timing.

These observations raise an interesting problem: that the Mairs Cave record, which is sensitive to recharge, appears to be hydrologically out of tune with the evidence in the marine record. We explore three possibilities for the disagreement in the marine and terrestrial records:

I. Sea surface temperatures (SSTs) in the Southern Ocean were more important for moisture delivery rather than mean latitudinal position of the westerlies;

II. the water balance was sensitive to temperature (i.e. evaporation) rather than simply rainfall (5.2.3); or

III. rainfall to Mairs Cave was dependent on another moisture source other than the westerlies (5.2.4).

Addressing the first point, we note that the $\sim 4\,^{\circ}\mathrm{C}$ rise in MD03-2611 SST from 18 to 16 ka (Fig. 6c) would boost the moisture originating from the Southern Ocean, possibly providing a relative increase in rainfall even if the MD03-2611 record implies that air masses from the Southern Ocean crossed the Flinders Ranges less frequently. However, the SST rise does not commence until 18 ka, ~ 1000 years later than the shift to increased recharge in the Flinders Ranges commencing at 18.9 ka. Additionally, SSTs stay high for the remainder of the record, whereas the Mairs Cave stalagmites provide strong support for a shift to aridity at 15.8 ka. These two observations argue against Southern Ocean SSTs being a primary driver.

5.2.3 Increased recharge due to reduced evapotranspiration

Addressing the second point, it was shown previously (Williams et al., 2006) that recharge to the Flinders Ranges at the LGM could be enhanced simply because evaporation would be reduced in a cooler environment (Williams et al., 2006). We demonstrate this also by using the Thornthwaite method to estimate evaporation (Thornthwaite, 1948). Figure 1c shows calculations of monthly hydrologically effective precipitation (HEP) for (i) present-day monthly rainfall and temperature in the Flinders Ranges and (ii) LGM temperatures, whereby monthly temperature was offset by $-6\,^{\circ}\mathrm{C}$ and $-10\,^{\circ}\mathrm{C}$, consistent with a range of estimates given for LGM temperature lowering in southern Australia (Galloway, 1965; Miller et al., 1997). Although simplistic, this calculation demonstrates the potential for a significant increase in recharge when potential evaporation is lowered (between 4- and 6-fold) with potential recharge occurring at 25–50 % of today's monthly rainfall. This further suggests that there is opportunity for recharge to be generated by lower magnitude events. That is, given that monthly recharge typically occurs via infrequent events, it suggests recharge could be generated at the LGM by events that are approximately half the magnitude required for recharge today, which would also occur more frequently. However, terrestrial temperatures were likely cooler through the whole of the LGM period. This explanation could be responsible for the presence of speleothem growth throughout the 23–16 ka period, but does not appear consistent with the relatively abrupt shift to enhanced recharge at 18.9 ka, which requires an additional mechanism.

5.2.4 Comparison of Mairs Cave record with tropical archives

Thirdly, we consider whether effective precipitation may be higher if the region is being watered from systems other than the westerlies. There is evidence that northern Australia and southern Indonesia were wetter during parts of the Last Termination and this has been linked to changes in the Indo-Australian summer monsoon (IASM) activity/Western Pacific Warm Pool (WPWP) dynamics and/or a southward shift in the Intertropical Convergence Zone (ITCZ) (e.g. Nott and Price, 1994; English et al., 2001; Turney et al., 2004; Denniston et al., 2013a; Ayliffe et al., 2013). A more southerly displaced ITCZ could increase the availability of tropical moisture into northern Australia, as was demonstrated in a modelling study under HS1 boundary conditions (Mohtadi et al., 2014). This could have increased the availability of tropically sourced moisture to the mid-latitudes via continental troughs as described in Sect. 2.

Figure 6 shows the speleothem records from Ball Gown Cave in NW Western Australia (Denniston et al., 2013a), Cape Range in Western Australia (Denniston et al., 2013b) and Liang Luar in Flores, Indonesia (Ayliffe et al., 2013), as well as marine record SO189-39KL of reconstructed tropical eastern Indian Ocean salinity, from the northern Mentawai Basin, off the coast of Sumatra (Mohtadi et al., 2014) (see Fig. 1a for locations). Both the Ball Gown Cave and Liang Luar records are considered to be influenced by the intensity/location of the IASM with a more southerly displaced IASM inferred during HS1 (Denniston et al., 2013; Ayliffe et al., 2013). While it is difficult to judge against the Ball Gown Cave record, given that the uncertainty in its chronology is approximately ± 1 kyr at this point, $\delta^{18}\mathrm{O}$ decreases at the onset of HS1 and rises again after 15 ka (Fig. 6f), which is approximately similar in timing to the period of highest recharge in the Mairs Cave record: 17.2 ± 0.08 (or possibly ~ 0.4 kyr earlier, given MC-S1's earliest growth was not retrieved) until 15.8 ± 0.07 ka. This interval also compares well with low $\delta^{18}\mathrm{O}$ from 17.6 ± 0.1 to 14.6 ± 0.1 ka in the comparatively well-dated Flores record. It also agrees well, in terms of timing, with events recorded in other precisely dated archives outside of the Australasian region, interpreted as a response to HS1 (e.g. Wang et al., 2001; Partin et al., 2007; Cheng et al., 2010) summarised in Naafs et al. (2013). Thus, there is consistent evidence that the enhanced recharge

recorded during ~ 17.2–15.8 ka at Mairs Cave coincides with a more southerly displaced IASM during HS1.

The above offers an explanation for the period of enhanced recharge seen in the Mairs Cave record during HS1. However, in the Mairs Cave record, this period of enhanced recharge occurred within the context of an earlier shift to relatively wetter conditions at 18.9 ka, evidenced by the decrease in speleothem $\delta^{18}O$ and $\delta^{13}C$, reduced isotopic disequilibrium, calcite fabric changes, and lowered Mg / Ca. According to the above studies, the timing of the ITCZ displacement coincides with the onset of HS1, which is at least 1000 years later than the onset of the relatively wetter interval at Mairs Cave (18.9 ka), although consistent with the highest interval of recharge in the MC-S1 record (17.2–15.8 ka), as described above. The Cape Range speleothem $\delta^{18}O$ record contains a downward trend that indicates increased recharge from approximately 19 ka that reaches a maximum during HS1 (Fig. 6g), consistent with the Mairs Cave record. This could support both sites being affected by a common driver. At Cape Range, the driver of $\delta^{18}O$ variability was unconstrained as this location is currently watered by moisture both from subtropical/tropical systems and mid-latitude westerlies, and these end members could not be separated isotopically (Denniston et al., 2013b). But given that both sites are receiving more recharge, and if the westerlies are further south during this interval as interpreted in the MD03-2611 record (Fig. 6b), it could be argued that a moisture source from lower latitudes is the most plausible explanation.

In the modern record, the delivery of moisture from the warm seas surrounding northern Australia to its interior is strongly governed by tropical ocean patterns associated with the El Niño–Southern Oscillation (ENSO) and the Indian Ocean Dipole (IOD) (Ummenhofer et al., 2009). Variability in tropical Pacific and Indian Ocean SSTs, in particular, strongly influences southern Australian rainfall (Ummenhofer et al., 2009; Pook et al., 2014) and has been shown to display decadal variability (Ummenhofer et al., 2011). A more La Niña-like state in the glacial period has been previously invoked (e.g. Sarnthein et al., 2011; Muller et al., 2008). However, a reconstruction of tropical eastern Indian Ocean salinity, from marine sediments off the coast of Sumatra, suggests anomalously dry conditions prevailed from approximately 19–20 until 16 ka (Mohtadi et al., 2014; Fig. 6h). This site lies within the core of the IOD zone of upwelling, suggesting that it is unlikely that the IOD was responsible for enhanced recharge to Mairs Cave from 18.9 to 15.8 ka. In the study by Mohtadi et al. (2014), the strong anti-phase relationship between hydroclimate records from NW and SE Indonesia (reduced rainfall over Sumatra versus enhanced rainfall over Flores) was noted and reproduced in their model simulation. This was argued to further support the southward position of the ITCZ during HS1. Interestingly, in the Sumatran record, this drying trend appears to begin as early as some time between 19 and 20 ka (Fig. 6h).

An alternative explanation is that a weaker subtropical ridge across Australia may have permitted deeper penetration of troughs into interior Australia. This possibility is supported by a modelling study by Sime et al. (2013), who showed that the strength of the Hadley cell in the subsidence regions was reduced during the LGM. Thus recharge to Mairs Cave throughout the 23–15.8 ka period may have been favoured by a weakened subtropical ridge, with a further enhancement of moisture delivery by a southward displaced ITCZ during HS1.

Finally, we consider the relationship between the Mairs Cave record and regional data for the transition to drier conditions at 15.8 ka in the Mairs Cave record. As noted by Zhang et al. (2016), both the Flores and Ball Gown Cave records have low $\delta^{18}O$ troughs at 16 ka, implying wet conditions, but the trend in both records quickly reverses, suggesting a weakening of the IASM followed from 16 to approximately 14.7 ka (Fig. 6f–g). The MD03-2611 marine record also suggests a northward displacement in the mid-latitude westerlies from 16 ka, implying a return of westerly airflow to the Flinders Ranges at the same time that Mairs Cave records an abrupt shift from wetter to drier conditions (Sect. 5.1.3). This combined evidence reinforces a tropical driver for enhanced recharge to the Flinders Ranges followed by an abrupt shift to aridity via the retraction of tropical moisture and restored westerly airflow. This feature in the Mairs Cave record is thus further evidence for the northward shift in the ITCZ interpreted in the monsoon speleothem records at the onset of the Bølling–Allerød (Ayliffe et al., 2013; Denniston et al., 2013a).

6 Conclusions

Two stalagmites from Mairs Cave, Flinders Ranges, are interpreted to record shallow groundwater recharge to the over the LGM/early deglacial. Relative recharge is primarily indicated by the on/off activation of speleothem growth and degree of isotopic disequilibrium, supported by Mg / Ca values and calcite fabric changes. It appears that this interval, overall, was relatively wetter than previous or subsequent times, with the wettest phase between 18.9 and 15.8 ka, ending abruptly with a shift to drier conditions at 15.8 ka. Specifically, we have identified three phases within the 23–15 ka interval, summarised as follows:

I. 23–18.9 ka: MC-S2 activates but shows isotopic disequilibrium driven by evaporation in the soil/epikarst water stores, punctuated with multi-decadal periods of higher effective recharge and cave flooding.

II. 18.9–15.8 ka: MC-S2 has reduced isotopic disequilibrium, indicating increased infiltration and/or reduced evapotranspiration and MC-S1 activates due to relatively more recharge. Speleothem $\delta^{13}C$ is also relatively lower in each record, supporting enhanced soil bioproductivity in wetter/warmer soils above Mairs Cave.

III. 15.8 ka: MC-S1 records a shift to aridity, coinciding with the termination of MC-S2 and, eventually, MC-S1 growth, indicating the end of effective recharge.

These findings agree well with other regional geomorphic evidence for high-magnitude floods of approximately centennial frequency in the Flinders silts (coinciding with phase I), lake highstands (coinciding with phase II), and re-activation of dunefields (overlapping phase III) in the southern Australian drylands. In comparison, the Mairs Cave record is the most precisely dated and highest-resolution record of these archives to date, and the first able to confirm that recharge to this region is responding to key global events during the Last Termination (LGM and HS1).

The source of moisture responsible for enhanced recharge could not be reliably isotopically fingerprinted for the Mairs Cave record, as it is within the hydrological uncertainty of the speleothem $\delta^{18}O$ data. However, comparing the Mairs Cave record with other records from further afield, notably the MD03-2611 marine record (westerly winds) and northwest Australian and Indonesian speleothem records (tropical systems), raises an intriguing possibility that wetter intervals in the southern Australian drylands appear to be more sensitive to the availability of tropical moisture rather than the position of the westerly winds. Thus it appears that westerly rainfall may have been relatively ineffectual at driving recharge to southern Australia during the LGM. The latter challenges simple assumptions made previously in the geomorphology and Quaternary literature that wetter intervals in the interior of southern Australian paleo-record during the last glacial imply westerly airflow as a driver (e.g. Cohen et al., 2012; Haberlah et al., 2010; Fitzsimmons et al., 2013).

The spectral analysis reveals that episodes of recharge to Mairs Cave occurred in approximately 180-year cycles that persisted through the whole 23–16 ka interval. This suggests that the mechanism for multi-centennial variability in recharge was operating throughout this period. This may be due to a weakened subtropical ridge with other mechanisms amplifying recharge from 18.9 ka, particularly during HS1. For example, Southern Ocean SSTs, reduced evapotranspiration, a further increase in availability of tropical moisture from a more southerly displaced ITCZ during HS1, or some combination of these. A future modelling study investigating these factors is warranted, as are further data from this region. In particular, high-resolution terrestrial reconstructions for the LGM/deglaciation period from higher latitudes that are more sensitive to the westerly winds and less influenced by tropically sourced moisture, e.g. southwest Western Australia and western Tasmania, are warranted.

Data availability. Stable isotope data from Fig. 3 are available from the NOAA Paleoclimatology database (https://www.ncdc.noaa.gov/data-access/paleoclimatology-data/datasets/speleothem).

The Supplement related to this article is available online at https://doi.org/10.5194/cp-13-667-2017-supplement.

Author contributions. Pauline C. Treble performed the stable isotope analyses for MC-S1 and the trace element analyses for both stalagmites as well as the majority of the data interpretation and manuscript drafting; John C. Hellstrom performed the U / Th dating; Silvia Frisia and Andrea Borsato performed the fabric log and thin section analysis; Linda K. Ayliffe collected the speleothems; Alan D. Griffiths drafted Figs. 1d and 5; Andrea Baker, Timothy J. Cohen, Michael K. Gagan and Russell N. Drysdale contributed to the interpretation and manuscript writing.

Competing interests. The authors declare that they have no conflict of interest.

Acknowledgements. We would like to thank Rod Wells for the use of stalagmite MC-S2 and discussions about Mairs Cave; James Shulmeister, Pandora Hope, John Chappell, Ed Rhodes, Martin Williams, Ian Houshold, and David Haberlah for discussions on the region's climate (both today and in the past) and geomorphology; and Monika Markowska for discussions on semi-arid speleothem records. We thank also Janece McDonald, Islay Laird, Krista Simon, and Joan Cowley for assistance with milling and isotope analysis; Stuart Hankin for drafting Fig. 1a, b; Patrick De Deckker, Matthias Moros, and Rhawn Denniston for supplying published data; and Dan Sinclair for discussions on quantifying PCP. We also thank the four anonymous reviewers, who provided valuable feedback that improved this manuscript. The stable isotope measurements on MC-S1 and MC-S2 were supported by Australian Research Council LIEF grants LE0989624 and LE0668400, and U-Th age measurements by Australian Research Council LIEF grant LE0989067. The majority of the data were collected whilst Pauline C. Treble was a research fellow at the Australian National University. This paper is a contribution to the SHAPE IFG.

Edited by: Andrew Lorrey
Reviewed by: four anonymous referees

References

Asrat, A., Baker, A., Mohammed, M. U., Leng, M. J., Van Calsteren, P., and Smith, C.: A high-resolution multi-proxy stalagmite record from Mechara, Southeastern Ethiopia: palaeohydrological implications for speleothem palaeoclimate reconstruction, J. Quaternary Sci., 22, 53–63, 2007.

Ayalon, A., Bar-Mathews, M., and Sass, E.: Rainfall-recharge relationships within a karstic terrain within the Eastern Mediterranean semi-arid region, Israel: d18O and dD charateristics, J. Hydrol., 207, 18–30, 1998.

Ayliffe, L. K., Marianelli, P. C., McCulloch, M. T., Mortimeter, G. E., Hellstrom, J. C., Moriarty, K. C., and Wells, R. T.: 500 ka precipitation record from southeastern Australia: Evidence for interglacial relative activity, Geology, 26, 147–150, 1998.

Ayliffe, L. K., Gagan, M. K., Zhao, J.-X., Drysdale, R. N., Hellstrom, J. C., Hantoro, W. S., Griffiths, M. L., Scott-Gagan, H., St Pierre, E., Cowley, J. A., and Suwargadi, B. W.: Rapid interhemispheric climate links via the Australasian monsoon during the last deglaciation, Nat. Commun., 4, 2908, https://doi.org/10.1038/ncomms3908, 2013.

Baker, A. and Brunsdon, C.: Non-linearities in drip water hydrology: an example from Stump Cross Caverns, Yorkshire, J. Hydrol., 277, 151–163, 2003.

Baldini, J. U. L.: Morphologic and dimensional linkage between recently deposited speleothems and drip water from Browns Folly Mine, Wiltshire, England, J. Cave Karst Stud., 63, 83-90, 2001.

Bar-Matthews, M., Ayalon, A., Matthews, A., Sass, E., and Halicz, L.: Carbon and oxygen isotope study of the active water-carbonate system in a karstic Mediterranean cave: Implications for paleoclimate research in semiarid regions, Geochim. Cosmochim. Ac., 60, 337–347, 1996.

Belli, R., Borsato, A., Frisia, S., Drysdale, R. N., Maas, R., and Greig, A.: Investigating Mg and Sr hydrological significance through Sr isotopes and particulate elements analyses in stalagmites across the Lateglacial to Holocene transition, Geochim. Cosmochim. Ac., 199, 247–263, https://doi.org/10.1016/j.gca.2016.10.024, 2017.

Bestland, E. A. and Rennie, J.: Stable isotope record (δ^{18}O and δ^{13}C) of a Naracoorte Caves speleothem (Australia) from before and after the Last Interglacial, Alcheringa, Special Issue, 1, 19–29, 2006.

Borsato, A., Johnston, V. E., Frisia, S., Miorandi, R., and Corradini, F.: Temperature and altitudinal influence on karst dripwater chemistry: Implications for regional-scale palaeoclimate reconstructions from speleothems, Geochim. Cosmochim. Ac., 177, 275–297, https://doi.org/10.1016/j.gca.2015.11.043, 2016.

Borsato, A., Frisia, S., and Miorandi, R.: Carbon dioxide concentration in temperate climate caves and parent soils over an altitudinal gradient and its influence on speleothem growth and fabrics, Earth Surf. Proc. Landf., 40, 1158–1170, https://doi.org/10.1002/esp.3706, 2015.

Bowler, J. M. (Ed.): Quaternary climate and tectonics in the evolution of the Riverine Plain, southeastern Australia, ANU Press, Canberra, Australia, 1978.

Bowler, J. M. and Wasson, R. J.: Glacial age environments of inland Australia, in: Late Cainozoic palaeoclimates of the Southern Hemisphere, edited by: Vogel, J. C., Balkema, Rotterdam, 1984.

Bradley, C., Baker, A., Jex, C. N., and Leng, M. J.: Hydrological uncertainties in the modelling of cave drip-water d18O and the implications for stalagmite palaeoclimate recontructions, Quaternary Sci. Rev. 29, 2201–2214, 2010.

Broecker, W. and Putnam, A. E.: How did the hydrologic cycle respond to the two-phase mystery interval?, Quaternary Sci. Rev., 57, 17–25, 2012.

Callen, R. A.: Quaternary climatic cycles, Lake Millyera region, southern Strzelecki Desert, T. Roy. Soc. South Aust., 108, 163–173, 1984.

Cuthbert, M. O., Baker, A., Jex, C. N., Graham, P. W., Treble, P. C., Andersen, M. S., and Acworth, R. I.: Drip water isotopes in semi-arid karst: implications for speleothem paleoclimatology, Earth Planet. Sc. Lett., 395, 194–204, 2014a.

Cuthbert, M. O., Rau, G. C., Andersen, M. S., Roshan, H., Rutlidge, H., Marjo, C. E., Markowska, M., Jex, C. N., Graham, P. W., Mariethoz, G., Acworth, R. I., and Baker, A.: Evaporative cooling of speleothem drip water, Sci Rep-Uk, 4, 2014b.

Cheng, H., Edwards, R. L., Broecker, W. S., Denton, G. H., Kong, X., Wang, Y., Zhang, R., and Wang, X.: Ice age terminations, Science, 326, 248–252, 2010.

Cheng, H., Edwards, R. L., Shen, C. C., Polyak, V. J., Asmerom, Y., Woodhead, J., Hellstrom, J., Wang, Y. J., Kong, X. G., Spotl, C., Wang, X. F., and Alexander, E. C.: Improvements in Th-230 dating, Th-230 and U-234 half-life values, and U-Th isotopic measurements by multi-collector inductively coupled plasma mass spectrometry, Earth Planet. Sc. Lett., 371, 82–91, 2013.

Clark, P. U., Shakun, J. D., Baker, P. A., Bartlein, P. J., Brewer, S., Brook, E., Carlson, A. E., Cheng, H., Kaufman, D. S., Liu, Z. Y., Marchitto, T. M., Mix, A. C., Morrill, C., Otto-Bliesner, B. L., Pahnke, K., Russell, J. M., Whitlock, C., Adkins, J. F., Blois, J. L., Clark, J., Colman, S. M., Curry, W. B., Flower, B. P., He, F., Johnson, T. C., Lynch-Stieglitz, J., Markgraf, V., McManus, J., Mitrovica, J. X., Moreno, P. I., and Williams, J. W.: Global climate evolution during the last deglaciation, P. Natl. Acad. Sci. USA, 109, E1134–E1142, 2012.

Cohen, T. J., Nanson, G. C., Jansen, J. D., Jones, B. G., Jacobs, Z., Treble, P., Price, D. M., May, J. H., Smith, A. M., Ayliffe, L. K., and Hellstrom, J. C.: Continenal aridification and the vanishing of Australia's megalakes, Geology, 39, 167–170, 2011.

Cohen, T. J., Nanson, G. C., Jansen, J. D., Jones, B. G., Jacobs, Z., Larsen, J. R., May, J. H., Treble, P., Price, D. M., and Smith, A. M.: Late Quaternary mega-lakes fed by the northern and southern river systems of central Australia: varying moisture sources and increased continental aridity, Palaeogeogr. Palaeocl., 356–357, 89–108, 2012.

Day, C. C. and Henderson, G. M.: Oxygen isotopes in calcite grown under cave-analogue conditions, Geoch. Cosmochim. Ac., 75, 3956–3972, https://doi.org/10.1016/J.Gca.2011.04.026, 2011.

De Boer, A. M., Graham, R. M., Thomas, M. D., Kohfeld, K. E.: The control of the Southern Hemisphere Westerlies on the position of the Subtropical Front, J. Geophys. Res.-Oceans, 118, 5669–5675, https://doi.org/10.1002/jgrc.20407, 2013.

De Deckker, P., Moros, M., Perner, K., and Jansen, E.: Influence of the tropics and southern westerlies on glacial interhemispheric asymmetry, Nat. Geosci., 5, 266–269, 2012.

Deininger, M., Fohlmeister, J., Scholz, D., and Mangini, A.: Isotope disequilibrium effects: The influence of evaporation and ventilation effects on the carbon and oxygen isotope composition of speleothems – A model approach, Geochim. Cosmochim. Ac., 96, 57–79, 2012.

Denniston, R. F., Wyrwoll, K. H., Asmerom, Y., Polyak, V. J., Humphreys, W. F., Cugley, J., Woods, D., LaPointe, Z., Peota, J., and Greaves, E.: North Atlantic forcing of millennial-scale Indo-Australian monsoon dynamics during the Last Glacial period, Quaternary Sci. Rev., 72, 159–168, 2013a.

Denniston, R. F., Asmerom, Y., Lachniet, M., Polyak, V. J., Hope, P., An, N., Rodzinyak, K., and Humphreys, W. F.: A Last Glacial Maximum through middle Holocene stalagmite record of coastal Western Australia climate, Quaternary Sci. Rev., 77, 101–112, 2013b.

Desmarchelier, J. M., Goede, A., Ayliffe, L. K., McCulloch, M. T., and Moriarty, K.: Stable isotope record and its palaeoenvironmental interpretation for a late Middle Pleistocene speleothem

from Victoria Fossil Cave, Naracoote, South Australia, Quaternary Sci. Rev., 19, 763–774, 2000.
Dreybrodt, W. and Deininger, M.: The impact of evaporation to the isotope composition of DIC in calcite precipitating water films in equilibrium and kinetic fractionation models, Geochim. Cosmochim. Ac., 125, 433–439, 2014.
Duan, W. H., Ruan, J. Y., Luo, W. J., Li, T. Y., Tian, L. J., Zeng, G. N., Zhang, D. Z., Bai, Y. J., Li, J. L., Tao, T., Zhang, P. Z., Baker, A., and Tan, M.: The transfer of seasonal isotopic variability between precipitation and drip water at eight caves in the monsoon regions of China, Geochim. Cosmochim. Ac., 183, 250–266, 2016.
English, P., Spooner, N. A., Chappell, J., Questiaux, D. G., and Hill, N. G.: Lake Lewis basin, central Australia: environmental evolution and OSL chronology, Quaternary Int., 83–85, 81–101, 2001.
Fairchild, I. J. and Baker, A.: Speleothem Science: From process to past environments, Wiley-Blackwell, Oxford, 2012.
Fairchild, I. J. and Treble, P. C.: Trace elements in speleothems as recorders of environmental change, Quaternary Sci. Rev., 28, 449–468, 2009.
Fantidis, J. and Ehhalt, D.: Variations of the carbon and oxygen isotopic composition in stalagmites and stalactites: Evidence of non-equilibrium isotopic fractionation, Earth Planet. Sc. Lett., 10, 136–144, 1970.
Feng, W. M., Banner, J. L., Guilfoyle, A. L., Musgrove, M., and James, E. W.: Oxygen isotopic fractionation between drip water and speleothem calcite: A 10-year monitoring study, central Texas, USA, Chem. Geol., 304, 53–67, 2012.
Fischer, M. J. and Treble, P. C.: Calibrating climate-delta O-18 regression models for the interpretation of high-resolution speleothem delta O-18 time series, J. Geophys. Res.-Atmos., 113, D17103, https://doi.org/10.1029/2007JD009694, 2008.
Fitzsimmons, K. E., Magee, J. W., and Amos, K. J.: Characterisation of aeolian sediments from the Strzelecki and Tirari Deserts, Australia: Implications for reconstructing palaeoenvironmental conditions, Sediment Geol., 218, 61–73, 2009.
Fitzsimmons, K. E., Cohen, T. J., Hesse, P. P., Jansen, J., Nanson, G. C., May, J. H., Barrows, T. T., Haberlah, D., Hilgers, A., Kelly, T., Larsen, J., Lomax, J., and Treble, P.: Late Quaternary palaeoenvironmental change in the Australian drylands, Quaternary Sci. Rev., 74, 78–96, 2013.
Fitzsimmons, K. E., Stern, N., Murray-Wallace, C. V., Truscott, W., and Pop, C.: The Mungo Mega-Lake Event, Semi-Arid Australia: Non-Linear Descent into the Last Ice Age, Implications for Human Behaviour, Plos One, 10, e0127008, https://doi.org/10.1371/journal.pone.0127008, 2015.
Frisia, S.: Microstratigraphic logging of calcite fabrics in speleothems as tool for palaeoclimate studies, Int. J. Speleol., 44, 1–16, 2015.
Frisia, S., Borsato, A., Fairchild, I. J., and McDermott, F.: Calcite fabrics, growth mechanisms and environments of formation in speleothems (Italian Alps and SW Ireland), J. Sediment. Res., 70, 1183–1196, 2000.
Fuller, L., Baker, A., Fairchild, I. J., Spötl, C., Marca-Bell, A., Rowe, P., and Dennis, P. F.: Isotope hydrology of dripwaters in a Scottish cave and implications for stalagmite palaeoclimate research, Hydrol. Earth Syst. Sci., 12, 1065–1074, https://doi.org/10.5194/hess-12-1065-2008, 2008.
Galloway, R. W.: Late Quaternary climates in Australia, J. Geol., 73, 603–618, 1965.
Gasse, F., Chalie, F., Vincens, A., Williams, M. A. J., and Williamson, D.: Climatic patterns in equatorial and southern Africa from 30,000 to 10,000 years ago reconstructed from terrestrial and near-shore proxy data, Quaternary Sci. Rev., 27, 2316–2340, 2008.
Goede, A., McCulloch, M., McDermott, F., and Hawkesworth, C.: Aeolian contribution to strontium and strontium isotope variations in a Tasmanian speleothem, Chem. Geol., 149, 37–50, 1998.
Gonzalez, L. A., Carpenter, S. J., and Lohmann, K. C.: Inorganic calcite morphology: roles of fluid chemistry and fluid flow, J. Sediment. Res., 62, 382–399, 1992.
Griffiths, M. L., Drysdale, R. N., Gagan, M. K., Frisia, S., Zhao, J., Ayliffe, L. K., Hantoro, W. S., Hellstrom, J. C., Fischer, M. J., Feng, Y., and Suwargadi, B. W.: Evidence for Holocene changes in Australian-Indonesian monsoon rainfall from stalagmite trace element and stable isotope ratios, Earth Planet. Sc. Lett., 292, 27–38, 2009.
Griffiths, M. L., Kimbrough, A. K., Gagan, M. K., Drysdale, R. N., Cole, J. E., Johnson, K. R., Zhao, J. X., Cook, B. I., Hellstrom, J. C., and Hantoro, W. S.: Western Pacific hydroclimate linked to global climate variability over the past two millennia, Nat. Commun., 7, 11719, https://doi.org/10.1038/ncomms11719, 2016.
Haberlah, D., Williams, M. A. J., Halverson, G., McTainsh, G. H., Hill, S. M., Hrstka, T., Jaime, P., Butcher, A. R., and Glasby, P.: Loess and floods: High-resolution multi-proxy data of Last Glacial Maximum (LGM) slackwater deposition in the Flinders Ranges, semi-arid South Australia, Quaternary Sci. Rev., 29, 2673–2693, 2010.
Hellstrom, J.: U-Th dating of speleotherns with high initial Th-230 using stratigraphical constraint, Quat. Geochronol., 1, 289–295, 2006.
Henderson, G. M.: Caving in to new chronologies, Science, 313, 620–622, 2006.
Hellstrom, J.: Rapid and accurate U/Th dating using parallel ion-counting multi-collector ICP-MS, J. Anal. Atom. Spectrom., 18, 1346–1351, 2003.
Hendy, C.: The isotope geochemistry of speleothems-I. The calculation of the effects of different modes of formation on the isotopic composition of speleothems and their applicability as palaeoclimatic indicators, Geochim. Cosmochim. Ac., 35, 802–824, 1971.
Hendy, C. and Wilson, A.: Palaeoclimatic data from speleothems, Nature, 219, 48–51, 1968.
Hendy, E. J., Tomiak, P. J., Collins, M. J., Hellstrom, J., Tudhope, A. W., Lough, J. M., and Penkman, K. E. H.: Assessing amino acid racemization variability in coral intra-crystalline protein for geochronological applications, Geochim. Cosmochim. Ac., 86, 338–353, 2012.
Hesse, P. P., Magee, J. W., and van der Kaars, S.: Late Quaternary climates of the Australian arid zone: a review, Quaternary Int., 118, 87–102, 2004.
Hill, A. L.: Mairs Cave Buckalowie Creek, Australian Speleological Federation map no. 5F3-CEG1009, 1958.
IAEA/WMO: Global Network of Isotopes in Precipitation, The GNIP Database, available at: http://www.iaea.org/water (last access: 22 June 2010), 2006.

Kalnay, E., Kanamitsu, M., Kistler, R., Collins, W., Deaven, D., Gandin, L., Iredell, M., Saha, S., White, G., Woollen, J., Zhu, Y., Leetmaa, A., Reynolds, R., Chelliah, M., Ebisuzaki, W., Higgins, W., Janowiak, J., Mo, K. C., Ropelewski, C., Wang, J., Jenne, R., and Joseph, D.: The NCEP/NCAR 40-Year Reanalysis Project, B. Am. Meteorol. Soc., 77, 437–471, 1996.

Kemp, J. and Rhodes, E. J.: Episodic fluvial activity of inland rivers in southeastern Australia: Palaeochannel systems and terraces of the Lachlan River, Quaternary Sci. Rev., 29, 732–752, 2010.

Kohfeld, K. E., Graham, R. M., de Boer, A. M., Sime, L. C., Wolff, E. W., Le Quere, C., and Bopp, L.: Southern Hemisphere westerly wind changes during the Last Glacial Maximum: paleo-data synthesis, Quaternary Sci. Rev., 68, 76–95, 2013.

Kraehenbuehl, P. Lawrence, R. E., and Flavel, S.: Caves of the Flinders Ranges. Cave Exploration Group of South Australia Occasional Paper No 9, 57 pp., 1997.

Luly, J. G.: On the equivocal fate of Late Pleistocene Callitris Vent. (Cupressaceae) woodlands in arid South Australia, Quaternary Int., 83–85, 155–168, https://doi.org/10.1016/S1040-6182(01)00037-4, 2001.

Markowska, M., Baker, A., Treble, P. C., Andersen, M. S., Hankin, S., Jex, C. N., Tadros, C. V., and Roach, R.: Unsaturated zone hydrology and cave drip discharge water response: Implications for speleothem paleoclimate record variability, J. Hydrol., 529, 662–675, https://doi.org/10.1016/j.jhydrol.2014.12.044, 2015.

Markowska, M., Baker, A., Andersen, M. S., Jex, C. N., Cuthbert, M. O., Rau, G. C., Graham, P. W., Rutlidge, H., Mariethoz, G., Marjo, C. E., Treble, P. C., and Edwards, N.: Semi-arid zone caves: Evaporation and hydrological controls on delta O-18 drip water composition and implications for speleothem paleoclimate reconstructions, Quaternary Sci. Rev., 131, 285–301, 2016.

Mickler, P. J., Stern, L. A., and Banner, J. L.: Large kinetic isotope effects in modern speleothems, Geol. Soc. Am. Bull., 118, 65–81, 2006.

Miller, G., Magee, J., and Jull, A.: Low-latitude glacial cooling in the Southern Hemisphere from amino-acid racemization in emu eggshells, Nature, 385, 241–244, 1997.

Moerman, J. W., Cobb, K. M., Partin, J. W., Meckler, A. N., Carolin, S. A., Adkins, J. F., Lejau, S., Malang, J., Clark, B., and Tuen, A. A.: Transformation of ENSO-related rainwater to dripwater δ18O variability by vadose water mixing, Geophys. Res. Lett., 41, 7907–7915, 2014.

Mohtadi, M., Prange, M., Oppo, D. W., De Pol-Holz, R., Merkel, U., Zhang, X., Steinke, S., and Luckge, A.: North Atlantic forcing of tropical Indian Ocean climate, Nature, 509, 76–80, https://doi.org/10.1038/nature13196, 2014.

Muller, J., Kylander, M., Wust, R. A. J., Weiss, D., Martinez-Cortizas, A., LeGrande, A. N., Jennerjahn, T., Behling, H., Anderson, W. T., and Jacobson, G.: Possible evidence for wet Heinrich phases in tropical NE Australia: the Lynch's Crater deposit, Quaternary Sci. Rev., 27, 468–475, 2008.

Naafs, B., Hefter, J., and Stein, R.: Millennial-scale ice rafting events and Hudson Strait Heinrich (-like) Events during the late Pliocene and Pleistocene: a review, Quaternary Sci. Rev., 80, 1–28, 2013.

Nott, J. and Price, D.: Plunge Pools and Paleoprecipitation, Geology, 22, 1047–1050, 1994.

Pape, J. R., Banner, J. L., Mack, L. E., Musgrove, M., and Guilfoyle, A.: Controls on oxygen isotope variability in precipitation and cave drip waters, central Texas, USA, J. Hydrol., 385, 203–215, 2010.

Partin, J. W., Cobb, K. M., Adkins, J. F., Clark, B., and Fernandez, D. P.: Millennial-scale trends in west Pacific warm pool hydrology since the Last Glacial Maximum, Nature, 449, 452–455, https://doi.org/10.1038/nature06164, 2007.

Pearce, N. J. G., Perkins, W. T., Westgate, J. A., Gorton, M. P., Jackson, S. E., Neal, C. R., and Chenery, S. P.: A compilation of new and published major and trace element data for NIST SRM 610 and NIST SRM 612 glass reference materials, Geostandards Newsletter, 21, 115–144, 1996.

Pietsch, T. J., Nanson, G. C., and Olley, J. M.: Late Quaternary changes in flow-regime on the Gwydir distributive fluvial system, southeastern Australia, Quaternary Sci. Rev., 69, 168–180, 2013.

Pook, M. J., Risbey, J. S., Ummenhofer, C. C., Briggs, P. R., and Cohen, T. J.: A synoptic climatology of heavy rain events in the Lake Eyre and Lake Frome catchments, Frontiers in Environmental Science, 2, 1–8, 2014.

Press, W. H. and Rybicki, G. B.: Fast algorithm for spectral analysis of unevenly sampled data, Astrophys. J., 338, 277–280, 1989.

Quigley, M. C., Horton, T., Hellstrom, J. C., Cupper, M. L., and Sandiford, M.: Holocene climate change in arid Australia from speleothem and alluvial records, Holocene, 20, 1093–1104, 2010.

Rau, G. C., Cuthbert, M. O., Andersen, M. S., Baker, A., Rutlidge, H., Markowska, M., Roshan, H., Marjo, C. E., Graham, P. W., and Acworth, R. I.: Controls on cave drip water temperature and implications for speleothem-based paleoclimate reconstructions, Quaternary Sci. Rev., 127, 19–36, 2015.

Riechelmann, D. F. C., Schroder-Ritzrau, A., Scholz, D., Fohlmeister, J., Spotl, C., Richter, D. K., and Mangini, A.: Monitoring Bunker Cave (NW Germany): A prerequisite to interpret geochemical proxy data of speleothems from this site, J. Hydrol., 409, 682–695, 2011.

Riechelmann, D. F. C., Deininger, M., Scholz, D., Riechelmann, S., Schroder-Ritzrau, A., Spotl, C., Richter, D. K., Mangini, A., and Immenhauser, A.: Disequilibrium carbon and oxygen isotope fractionation in recent cave calcite: Comparison of cave precipitates and model data, Geochim. Cosmochim. Ac., 103, 232–244, 2013.

Risbey, J. S., Pook, M. J., McIntosh, P. C., Ummenhofer, C. C., and Meyers, G.: Characteristics and variability of synoptic features associated with cool season rainfall in southeastern Australia, Int. J. Climatol., 29, 1595–1613, 2009.

Rutlidge, H., Baker, A., Marjo, C. E., Andersen, M. S., Graham, P. W., Cuthbert, M. O., Rau, G. C., Roshan, H., Markowska, M., Mariethoz, G., and Jex, C. N.: Dripwater organic matter and trace element geochemistry in a semi-arid karst environment: Implications for speleothem paleoclimatology, Geochim. Cosmochim. Ac., 135, 217–230, 2014.

Sarnthein, M., Grootes, P. M., Holbourn, A., Kuhnt, W., and Kuhn, H.: Tropical warming in the Timor Sea led deglacial Antarctic warming and atmospheric CO2 rise by more than 500 yr, Earth Planet Sc. Lett., 302, 337–348, 2011.

Scholz, D., Hoffmann, D. L., Hellstrom, J., and Ramsey, C. B.: A comparison of different methods for speleothem age modelling, Quat. Geochronol., 14, 94–104, 2012.

Schwerdtfeger, P. and Curran, E. (Eds.): Climate of the Flinders Ranges, Royal Society of South Australia, Adelaide, 1996.

Self, C. A. and Hill, C. A.: How speleothems grow: an introduction to the ontogeny of cave minerals, J. Cave Karst Stud., 65, 130–151, 2003.

Shulmeister, J., Goodwin, I., Renwick, J., Harle, K., Armand, L., McGlone, M. S., Cook, E., Dodson, J., Hesse, P. P., Mayewski, P., and Curran, M.: The Southern Hemisphere westerlies in the Australasian sector over the last glacial cycle: a synthesis, Quaternary Int., 118, 23–53, 2004.

Shulmeister, J., Kemp, J., Fitzsimmons, K. E., and Gontz, A.: Constant wind regimes during the Last Glacial Maximum and early Holocene: evidence from Little Llangothlin Lagoon, New England Tablelands, eastern Australia, Clim. Past, 12, 1435–1444, https://doi.org/10.5194/cp-12-1435-2016, 2016.

Sime, L. C., Kohfeld, K. E., Le Quere, C., Wolff, E. W., de Boer, A. M., Graham, R. M., and Bopp, L.: Southern Hemisphere westerly wind changes during the Last Glacial Maximum: model-data comparison, Quaternary Sci. Rev., 64, 104–120, 2013.

Sinclair, D. J., Banner, J. L., Taylor, F. W., Partin, J., Jenson, J., Mylroie, J., Goddard, E., Quinn, T., Jocson, J., and Miklavic, B.: Magnesium and strontium systematics in tropical speleothems from the Western Pacific, Chem. Geol., 294, 1–17, 2012.

Singh, G. and Luly, J.: Changes in Vegetation and Seasonal Climate since the Last Full Glacial at Lake Frome, South-Australia, Palaeogeogr. Palaeocl., 84, 75–79, 1991.

Stoll, H. M., Moreno, A., Mendez-Vicente, A., Gonzalez-Lemos, S., Jimenez-Sanchez, M., Dominguez-Cuesta, M. J., Edwards, R. L., Cheng, H., and Wang, X. F.: Paleoclimate and growth rates of speleothems in the northwestern Iberian Peninsula over the last two glacial cycles, Quaternary Res., 80, 284–290, 2013.

St Pierre, E., Zhao, J. X., Feng, Y. X., and Reed, E.: U-series dating of soda straw stalactites from excavated deposits: method development and application to Blanche Cave, Naracoorte, South Australia, J. Archaeol. Sci., 39, 922–930, 2012.

Thornthwaite, C. W.: An approach toward a rational classification of climate, Geogr. Rev., 38, 55–94, 1948.

Treble, P., Shelley, J. M. G., and Chappell, J.: Comparison of high resolution sub-annual records of trace elements in a modern (1911–1992) speleothem with instrumental climate data from southwest Australia, Earth Planet. Sc. Lett., 216, 141–153, 2003.

Treble, P. C., Chappell, J., Gagan, M. K., McKeegan, K. D., and Harrison, T. M.: In situ measurement of seasonal delta O-18 variations and analysis of isotopic trends in a modem speleothem from southwest Australia, Earth Planet. Sc. Lett., 233, 17–32, 2005.

Treble, P. C., Bradley, C., Wood, A., Baker, A., Jex, C. N., Fairchild, I. J., Gagan, M. K., Cowley, J., and Azcurra, C.: An isotopic and modelling study of flow paths and storage in Quaternary aeolinite, SW Australia: implications for speleothem paleoclimate records, Quatarnary Sci. Rev., 64, 90–103, 2013.

Treble, P. C., Fairchild, I. J., Griffiths, A., Baker, A., Meredith, K. T., Wood, A., and McGuire, E.: Impacts of cave air ventilation and in-cave prior calcite precipitation on Golgotha Cave dripwater chemistry, southwest Australia, Quaternary Sci. Rev., 127, 61–72, 2015.

Treble, P. C., Fairchild, I. J., Baker, A., Meredith, K. T., Andersen, M. S., Salmon, S. U., Bradley, C., Wynn, P. M., Hankin, S., Wood, A., and McGuire, E.: Roles of forest bioproductivity, transpiration and fire in a nine-year record of cave dripwater chemistry from southwest Australia, Geochim. Cosmochim. Ac., 184, 132–150, 2016.

Tremaine, D. M. and Froelich, P. N.: Speleothem trace element signatures: A hydrologic geochemical study of modern cave dripwaters and farmed calcite, Geochim. Cosmochim. Ac., 121, 522–545, 2013.

Turgeon, S. and Lundberg, J.: Chronology of discontinuities and petrology of speleothems as paleoclimatic indicators of the Klamath Mountains, southwest Oregon, USA, Carbonate. Evaporite., 16, 153, https://doi.org/10.1007/BF03175833, 2001.

Turney, C. S. M., Kershaw, A. P., Clemens, S. C., Branch, N., Moss, P. T., and Fifield, L. K.: Millennial and orbital variations of El Nino/Southern Oscillation and high-latitude climate in the last glacial period, Nature, 428, 306–310, 2004.

Turney, C. S. M., Kershaw, A. P., Lowe, J. J., van der Kaars, S., Johnston, R., Rule, S., Moss, P., Radke, L., Tibby, J., McGlone, M. S., Wilmshurst, J. M., Vandergoes, M. J., Fitzsimons, S. J., Bryant, C., James, S., Branch, N. P., Cowley, J., Kalin, R. M., Ogle, N., Jacobsen, G., and Fifield, L. K.: Climatic variability in the southwest Pacific during the Last Termination (20–10 kyr BP), Quaternary Sci. Rev., 25, 886–903, 2006.

Ummenhofer, C. C., England, M. H., McIntosh, P. C., Meyers, G. A., Pook, M. J., Risbey, J. S., Gupta, A. S., and Taschetto, A. S.: What causes southeast Australia's worst droughts?, Geophys. Res. Lett., 36, L04706, https://doi.org/10.1029/2008gl036801, 2009.

Ummenhofer, C. C., Sen Gupta, A., Li, Y., Taschetto, A. S., and England, M. H.: Multi-decadal modulation of the El Nino-Indian monsoon relationship by Indian Ocean variability, Environ. Res. Lett., 6, 034006, https://doi.org/10.1088/1748-9326/6/3/034006, 2011.

Vaks, A., Bar-Matthews, M., Ayalon, A., Matthews, A., Frumkin, A., Dayan, U., Halicz, L., Almogi-Labin, A., and Schilman, B.: Paleoclimate and location of the border between Mediterranean climate region and the Saharo–Arabian Desert as revealed by speleothems from the northern Negev Desert, Israel. E.P.S.L. 249, 384–399, 2006.

Wang, X., Auler, A. S., Edwards, R. L., Cheng, H., Cristall, P. S., Smart, P. L., Richards, D. A., and Shen, C.-C.: Wet periods in northeastern Brazil over the past 210 kyr linked to distant climate anomalies, Nature, 432, 740–743, 2004.

Wang, Y. J., Cheng, H., Edwards, R. L., An, Z. S., Wu, J. Y., Shen, C. C., and Dorale, J. A.: A high-resolution absolute dated late Pleistocene monsoon record from Hulu Cave, China, Science, 294, 2345–2348, 2001.

Welker, J. M.: Isotopic ($d^{18}O$) characteristics of weekly precipitation collected across the USA: an initial analysis with application to water source studies, Hydrol. Process., 14, 1449–1464, 2000.

Williams, M., Nitschke, N., and Chor, C.: Complex geomorphic response to late Pleistocene climatic changes in the arid Flinders Ranges of South Australia, Geomorphologie, 2006, 249–258, 2006.

Williams, M., Cook, E., van der Kaars, S., Barrows, T. T., Shulmeister, J., and Kershaw, P.: Glacial and deglacial climatic patterns in Australia and surrounding regions from 35 000 to 10 000 years ago reconstructed from terrestrial and near-shore proxy data, Quaternary Sci. Rev., 28, 2398–2419, 2009.

Wyrwoll, K.-H., Dong, B., and Valdes, P.: On the position of southern hemisphere westerlies at the Last Glacial Maximum: an outline of AGCM simulation results and evaluation of their implications, Quaternary Sci. Rev., 19, 881–898, 2000.